

This is an Open Access document downloaded from ORCA, Cardiff University's institutional repository: <https://orca.cardiff.ac.uk/id/eprint/129903/>

This is the author's version of a work that was submitted to / accepted for publication.

Citation for final published version:

Mehrnegar, Nooshin, Jones, Owen , Singer, Michael Bliss , Schumacher, Maïke, Bates, Paul and Forootan, Ehsan 2020. Comparing global hydrological models and combining them with GRACE by dynamic model data averaging (DMDA). *Advances in Water Resources* 138 , 103528. 10.1016/j.advwatres.2020.103528

Publishers page: <http://dx.doi.org/10.1016/j.advwatres.2020.103528>

Please note:

Changes made as a result of publishing processes such as copy-editing, formatting and page numbers may not be reflected in this version. For the definitive version of this publication, please refer to the published source. You are advised to consult the publisher's version if you wish to cite this paper.

This version is being made available in accordance with publisher policies. See <http://orca.cf.ac.uk/policies.html> for usage policies. Copyright and moral rights for publications made available in ORCA are retained by the copyright holders.



1 Comparing Global Hydrological Models and Combining them  
2 with GRACE by Dynamic Model Data Averaging (DMDA)

3 Nooshin Mehrnegar<sup>a</sup>, Owen Jones<sup>b</sup>, Michael Bliss Singer<sup>a,c</sup>, Maike Schumacher<sup>d</sup>,  
4 Paul Bates<sup>e</sup>, Ehsan Forootan<sup>a,d</sup>

5 <sup>a</sup>*School of Earth and Ocean Sciences, Cardiff University, Cardiff CF103AT, UK*

6 <sup>b</sup>*School of Mathematics, Cardiff University, Cardiff CF244AG, UK*

7 <sup>c</sup>*Earth Research Institute, University of California Santa Barbara, Santa Barbara, 91306, USA*

8 <sup>d</sup>*Institute of Physics and Meteorology (IPM), University of Hohenheim, Stuttgart D70593,  
9 Germany*

10 <sup>e</sup>*School of Geographical Sciences, University of Bristol, University Road, Clifton, Bristol BS81SS,  
11 UK*

---

12 **Abstract**

13 Historically, hydrological models have been developed to represent land-atmosphere  
14 interactions by simulating water storage and water fluxes. These models, however,  
15 have their own unique characteristics (strength and weakness) in capturing different  
16 aspects of the water cycle, and their results are typically compared to or calibrated  
17 against in-situ observations such as river runoff measurements. As a result, there  
18 may be gross inaccuracies in the estimation of water storage states produced by  
19 these models. In this study, we present the novel approach of Dynamic Model Data  
20 Averaging (DMDA), which can be used to compare and merge multi-model water  
21 storage simulations with monthly Terrestrial Water Storage (TWS, a vertical summa-  
22 tion of surface and sub-surface water storage) estimates from the Gravity Recovery  
23 And Climate Experiment (GRACE) satellite mission. Here, the main hypothesis is  
24 that merging GRACE data with multi-model outputs likely provides more skillful  
25 hydrological estimations compared to a single model or data set. Theoretically, the  
26 proposed DMDA combines the benefits of the Kalman Filter (KF) and Bayesian  
27 Model Averaging (BMA) techniques and has the capability to deal with various ob-  
28 servations and models with different error structures. Based on the Bayes theory,  
29 DMDA provides time-variable weights for hydrological models to compute an aver-  
30 age of their outputs that are best fitted to GRACE TWS estimates. Numerically,  
31 the DMDA method is implemented by integrating the output of six hydrological and  
32 land surface models (PCR-GLOBWB, SURFEX-TRIP, LISFLOOD, HBV-SIMREG,  
33 W3RA, and ORCHIDEE) and monthly GRACE TWS estimates (2002–2012) within  
34 the world’s 33 largest river basins, while considering the inherent uncertainties of

35 all inputs. Our results indicate that DMDA correctly separates GRACE TWS es-  
36 timates into surface water, soil moisture and groundwater compartments. Linear  
37 trends fitted to the DMDA-derived groundwater compartment are found to be dif-  
38 ferent from those of original models. This means that anthropogenic influences within  
39 the GRACE data, which are not well reflected by models, are introduced by DMDA.  
40 We also find that temporal correlation coefficients between the DMDA-derived in-  
41 dividual water storage estimations (surface water, soil moisture, and groundwater)  
42 and the El Niño Southern Oscillation (ENSO) index are considerably increased com-  
43 pared to those derived between individual model simulations and ENSO (e.g., an  
44 increase from -0.2 to 0.6 in the Murray River Basin). For the Nile River Basin, they  
45 changed from 0.1 to 0.4 for the soil moisture, and from 0.3 to 0.7 for the surface wa-  
46 ter compartment. Comparisons between the DMDA-derived surface water and those  
47 from independent satellite altimetry observations indicate that after implementing  
48 DMDA, temporal correlation coefficients within major lakes are increased. Based on  
49 these results, we have gained confidence in the DMDA water storage estimates to be  
50 used for improving the characterization of water storage over broad regions of the  
51 globe.

52 *Keywords:* GRACE, Terrestrial Water Storage (TWS), Dynamic Model Data  
53 Averaging (DMDA), Kalman Filter (KF), Bayesian Model Averaging (BMA),  
54 Multi-Hydrological Models, Satellite Altimetry

---

## 55 1. Introduction

56 Studying global water storage changes and their relationships with climate vari-  
57 ability and exploring their trends are important to understand the interactions be-  
58 tween the Earth’s water, energy, and carbon cycles. It is also essential for managing  
59 water resources and understanding floods and food risks in a changing climate. In-  
60 situ and/or remote sensing observations provide estimates of different aspects of  
61 the Earth system, but they do not provide water cycle closure due to sampling  
62 and retrieval errors. In practice, hydrological models are used to quantify hydro-  
63 meteorological processes such as interactions between the global climate system and  
64 the water cycle (*Sheffield et al., 2012*), the contribution of land hydrology to global  
65 sea level rise (*Boening et al., 2012*), as well as to support applications related to wa-  
66 ter resources planning and management (*Hanington et al., 2017*). However, model  
67 simulations are prone to errors due to imperfect model structure, as well as errors in  
68 inputs and forcing data that are used to run model simulations. As a result, avail-  
69 able models operating at regional to global scales have limited skills to reflect human

70 impacts on water storage and runoff changes (*Wada et al., 2012; Scanlon et al., 2018;*  
71 *Singer et al., 2018*).

72 Among available remote sensing techniques, the Gravity Recovery And Climate  
73 Experiment (GRACE, 2002–2017) satellite mission (*Tapley et al., 2004*) and its  
74 Follow-On mission (GRACE-FO, 2018–onward) provide an opportunity to assess  
75 the global water cycle by monitoring time-variable gravity fields. Global GRACE-  
76 derived time-variable gravity field data can be used to estimate changes in Terrestrial  
77 Water Storage (TWS), which is a vertical summation of canopy, surface water (lakes,  
78 rivers, and wetlands), as well as soil moisture and groundwater storage. Changes in  
79 TWS provide a critical measure of regional and global water balances, which cannot  
80 be measured by any other satellite mission. A review of GRACE applications in  
81 hydrology, and particularly for groundwater monitoring, can be found in *Frappart*  
82 *and Ramillien (2018)*.

83 GRACE data can be used in conjunction with hydrological models to maximize  
84 information gained from modelling with rationalisation and separation of GRACE  
85 TWS. Thus, the gravimetric data from GRACE can inject realism into regional hy-  
86 drological predictions, which are often poorly constrained in terms of TWS. Generally  
87 speaking, integrating GRACE data with hydrological models is important from two  
88 perspectives: (1) it can update (modify) water storage simulation within hydrologi-  
89 cal models and (2) it vertically separates GRACE TWS into storage compartments.  
90 The first point is of interest for hydrologists since most global models are not usually  
91 combined with water storage observations (*Bai et al., 2018*). Therefore, such updates  
92 may lead to more realistic water storage simulations, which makes these models more  
93 useful for water resource applications (see e.g., *Werth et al., 2009; Mostafaie et al.,*  
94 *2018*). Regarding the second point, it is important to state that any attempt to  
95 vertically separate GRACE-derived TWS into its individual components requires a  
96 priori information from other sources, such as, hydrological models, satellite altime-  
97 try observations to estimate surface water storage, and soil moisture remote sensing  
98 data to estimate shallow depth soil moisture storage changes (*Forootan et al., 2014*).

99 Various studies have developed techniques to merge multi-resources and achieve  
100 vertical separation of surface and sub-surface water storage compartments by several  
101 methods outlined below.

102 (a) Forward modeling techniques are used to evaluate different compartments of  
103 mass variations through a simple reduction process, relying on model and/or observa-  
104 tion data for other compartments, e.g., surface water and soil moisture, if groundwa-  
105 ter should be estimated (e.g., *Tiwari et al., 2009; Rodell et al., 2009; Strassberg et al.,*  
106 *2009; Feng et al., 2013; Khandu et al., 2016*). This method is relatively straightfor-  
107 ward, but it is not necessarily the most accurate way to separate GRACE signals,

108 due to the reflection of modeling error and/or observation errors on the final estima-  
109 tion of mass changes. Also, the spatial and temporal resolution of the observations  
110 (from satellites or in-situ) and model outputs, as well as their signal content are not  
111 necessarily consistent (see the discussions in, e.g., [Forootan et al., 2014](#)). Most of  
112 these limitations are taken into account by the methods described in what follows.

113 (b) Statistical inversion techniques, which are formulated based on statistical sig-  
114 nal decomposition techniques, such as Principal Component Analysis (PCA, [Lorenz,](#)  
115 [1956](#)) and its alternatives, e.g., Independent Component Analysis (ICA, [Forootan](#)  
116 [and Kusche, 2012, 2013](#)), have been used in previous studies to separate GRACE  
117 TWS into individual water storage estimates. For example, [Schmeer et al. \(2012\)](#)  
118 used PCA to generate a priori information about mass changes from global ocean,  
119 atmosphere, and land hydrology models. Then, they applied a least squares tech-  
120 nique to use GRACE TWS to modify their priori estimates. A statistical inversion,  
121 which works based on both PCA and ICA, was proposed in [Forootan et al. \(2014,](#)  
122 [2017\)](#) and [Awange et al. \(2014\)](#) to separate GRACE TWS using auxiliary data of sur-  
123 face water from satellite altimetry and individual sub-surface water storage estimate  
124 from a land surface model (Global Land Data Assimilation System (GLDAS, [Rodell](#)  
125 [et al., 2004](#))). This inversion harmonizes the use of all available data sets within a  
126 single least squares framework. As a result, a more consistent mass estimate (than  
127 that of the forward modeling in (a)) for individual water storage components can be  
128 achieved.

129 (c) Data Assimilation (DA) as well as simultaneous Calibration/Data Assimila-  
130 tion (C/DA) have been used in recent years to merge GRACE data with hydrological  
131 model outputs or other types of observations. These techniques rely on the model  
132 equations to relate water and energy fluxes to water storage changes. Therefore,  
133 unlike the inversion approach (b), combining information from observations (e.g.,  
134 GRACE TWS estimates) and a model is performed in a physically justifiable way.  
135 DA or C/DA can potentially increase physical understanding of the model and im-  
136 prove the model states by decreasing the simulation errors. For example, DA is used  
137 in [Zaitchik et al. \(2008\)](#); [Giroto et al. \(2016, 2017\)](#); [Tian et al. \(2017\)](#); [Khaki et al.](#)  
138 [\(2018d,e\)](#), while C/DA is applied in [Schumacher et al. \(2016, 2018\)](#) to improve global  
139 models such as GLDAS ([Rodell et al., 2004](#)), World-Wide Water Resources Assess-  
140 ment (W3RA, [Van Dijk, 2010](#)), WaterGap Global Hydrological Model (WGHM, [Döll](#)  
141 [et al., 2003](#)), and NOAH Multi Parameterization Land Surface Model (NOAH-MP  
142 LSM, [Niu et al., 2011](#)). Most of the previous DA and C/DA are implemented region-  
143 ally (except [Van Dijk et al. \(2014\)](#); [Khaki et al. \(2017a, 2018a\)](#)) for example over the  
144 Mississippi River Basin ([Zaitchik et al., 2008](#); [Schumacher et al., 2016](#)), Bangladesh  
145 ([Khaki et al., 2018d](#)), the Middle East ([Khaki et al., 2018e](#)), and the Murray-Darling

146 River Basin (*Tian et al., 2017; Schumacher et al., 2018*). In addition, these studies  
147 rely on simulation from (only) one selected hydrological model, which could contain  
148 errors in the model structure such as biases in the model’s internal parameters and  
149 boundary conditions. In each of these studies, multiple realisations of the model-  
150 derived water storage simulations were generated by perturbing the input forcing  
151 data and/or model parameters. A sequential integration techniques such as the En-  
152 samble Kalman Filtering (EnKF, *Evensen, 1994*) or its extensions was then used to  
153 merge GRACE data with the (ensemble) outputs of a single model (e.g., *Schumacher*  
154 *et al., 2016, 2018; Khaki et al., 2017b*). *Van Dijk et al. (2014)* used EnKF to merge  
155 GRACE data with a priori data from models and other remote sensing techniques.  
156 Their study covered the period of 2003-2012 and focused on updating the individual  
157 water storage estimates rather than interpreting the water storage estimates in terms  
158 of trends or addressing the suitability of models used to perform the analyses.

159 (d) In recent years, Bayesian-based techniques have been used to combine differ-  
160 ent observations with models and update their outputs. For example, *Long et al.*  
161 *(2017)* applied the Bayesian Model Averaging (BMA, *Hsu et al., 2009*) technique to  
162 average multiple GRACE TWS products and global hydrological models to analyse  
163 spatial and temporal variability of global TWS. However, their study did not as-  
164 sess the update of individual surface and sub-surface water storage estimates. *Sha*  
165 *et al. (2018)* used a model-data synthesis framework based on Bayesian Hierarchical  
166 Modelling (BHM, see e.g., *Banerjee et al., 2004*) to use GRACE TWS estimates to  
167 update land surface deformations derived from Glacial Isostatic Adjustment (GIA)  
168 models. Their study did not, however, address global hydrological mass changes.

169 It is worth mentioning here that the Ensemble Kalman Filter used for DA and  
170 C/DA can also be classified as a Bayesian-based technique because the cost function  
171 for updating unknown state parameters condition on the measurement data, is for-  
172 mulated based on the Bayes theory (see e.g., *Evensen, 2003; Schumacher, 2016; Fang*  
173 *et al., 2018*). Methods, such as Particle Filter (PF) and Particle Smoother (PS) are  
174 also Bayesian (*Särkkä, 2013*), and have already been applied in a wide range of geo-  
175 physical and hydrological applications. For example, *Weerts and El Serafy (2006)*  
176 compared the capability of EnKF and PF to update a conceptual rainfall-runoff  
177 model using discharge and rainfall data. *Plaza Guingla et al. (2013)* also used the  
178 standard PF to assimilate a densely sampled discharge records into a conceptual  
179 rainfall-runoff model. However, *Bain and Crisan (2008)* and *Del Moral and Miclo*  
180 *(2000)* show that the rate of convergence of the approximate probability distribu-  
181 tion until attainment of the true posterior is inversely proportional to the number  
182 of particles used in the filter. This means that the filter perfectly approximates the  
183 posterior distribution when the number of particles tends to infinity. However, since

184 the computational cost of PF grows with the number of particles, choosing a specific  
185 number of particles in the design of filters is a key parameter for these methods. The  
186 rationale for introducing a new Bayesian data-model merging algorithm in this study  
187 is described in (e).

188 (e) In this study, we present the Dynamic Model Data Averaging method (DMDA,  
189 i.e., a modified version of Dynamic Model Averaging (DMA) approach presented by  
190 [Raftery et al., 2010](#)) to merge multi-model derived water storage simulations with  
191 GRACE TWS estimates, as an alternative technique to that described in (d). Our  
192 main goal is to evaluate available model outputs against GRACE TWS and merge  
193 them in a sensible way to gain more realistic insights about global surface and sub-  
194 surface water storage changes. The main hypothesis behind the presented approach is  
195 that each global hydrological model has its own unique characteristics and strengths  
196 in capturing different aspects of the water cycle. Therefore, relying on a single  
197 model often leads to predictions that represent some phenomena or events well at  
198 the expenses of others. [Scanlon et al. \(2018\)](#) recently compared GRACE TWS with  
199 the outputs of global models, whose results indicated inconsistencies in long-term  
200 trends and cyclic (e.g., seasonal) components. Besides, many studies have concluded  
201 that effective combination of multiple models may provide more skillful hydrological  
202 simulations compared to a single model ([Duan et al., 2007](#)). Therefore, a multi-model  
203 choice is considered in this study.

204 Our motivation to formulate the DMDA is based on its capability to deal with  
205 various observations and models with different structures. In summary, DMDA is  
206 based on the Bayes theory and provides time-variable weights to compute an average  
207 of hydrological model outputs, yielding the best fit to GRACE TWS estimates, while  
208 considering their errors (see section 3). These time-variable weights indicate which of  
209 the available models at a given point in time fits better to GRACE TWS estimates.  
210 These weights can then be used to separate the components of TWS and modify the  
211 estimation of water storage in these individual components. Therefore, the DMDA-  
212 derived ensemble is expected to yield more skillful (realistic) hydrological simulations  
213 compared to any individual model (see similar arguments in [Duan et al., 2007](#)). Here,  
214 we promote the use of DMDA over the previously introduced EnKF, PF, and PS  
215 methods because it is computationally more efficient in handling large dimensional  
216 problems such as the global integration implemented in this study. In addition, the  
217 DMDA's time-variable weights can be used to assess the performance of hydrological  
218 models, whereas this aspect is missing in other merging techniques. More details  
219 about the computational aspects of DMDA are provided in section 3.

220 To implement the DMDA method, surface and sub-surface water storage simu-  
221 lations of the six published global hydrological and land surface models ([Schellekens](#)

222 *et al.*, 2017) are used. These models are structurally different but they are all forced  
223 by the same reanalysis data set (WATCH-Forcing-Data-ERA-Interim, WFDEI *Wee-*  
224 *don et al.*, 2014) as inputs. GRACE-derived TWS estimates are then used in the  
225 DMDA method to compare their outputs and merge them. A challenging problem in  
226 merging GRACE TWS with the outputs from multiple hydrological models is related  
227 to their different spatial and temporal resolutions. To overcome the computational  
228 problem caused by the spatial and temporal mismatch, *Schumacher et al.* (2016)  
229 introduced spatial and temporal matching functions, which are able to avoid compu-  
230 tational problems. In this study, we did not implement the spatial/temporal operator  
231 because both model outputs and GRACE data were set at monthly (temporal) and  
232 basin-averaged (spatial). Handling the differences in spectral domain is described  
233 in section 2.2. A realistic synthetic example is presented in section 4.1 to test the  
234 performance of the DMDA method, where the true merged values are known and the  
235 method can be evaluated to provide the confidence that it can be applied to a real  
236 case study. Our numerical results cover the world’s 33 largest river basins (see Figure  
237 *ESM.1* in Electronic Supporting Material, ESM) for the period of 2002–2012, during  
238 which both GRACE data and model simulations are available. Global hydrological  
239 model outputs are compared against GRACE TWS, using DMDA-derived temporal  
240 weights, within the largest river basins for the period of this study (see section 4.2).  
241 The DMDA-derived updates, which are assigned to the long-term trend of surface  
242 and sub-surface water storage components, are explored and interpreted (see section  
243 4.3).

244 Among many climatic factors that influence inter-annual to decadal TWS changes,  
245 the El Niño Southern Oscillation (ENSO, *Barnston and Livezey*, 1987) events rep-  
246 resent a dominant impact on global precipitation and TWS changes (see, e.g., *Hurk-*  
247 *mans et al.*, 2009; *Chen et al.*, 2010; *Zhang et al.*, 2015; *Forootan et al.*, 2016; *Ni et al.*,  
248 2018; *Anyah et al.*, 2018; *Forootan et al.*, 2019). In this study, temporal correlation  
249 coefficients between model-derived storage outputs and the ENSO index are used as  
250 a measure to determine whether implementing the DMDA helps to derive realistic  
251 storage simulations (see section 4.3.1). In addition, independent surface water level  
252 observations from satellite altimetry within 14 major lakes, located in different river  
253 basins around the world, are used to validate our results (see section 4.4). This paper  
254 contains an Electronic Supporting Material (ESM) document that provide auxiliary  
255 information to improve understanding of the performed investigations.

## 256 2. Data sources

257 The data used in this paper include the monthly GRACE data to compute Terres-  
258 trial Water Storage (TWS) and individual water storage estimates from global models

259 to provide a priori estimates to perform a Bayesian signal separation. GRACE TWS  
260 estimates are used in the DMDA to modify the multi-model water storage outputs.

### 261 *2.1. GRACE Data*

262 The latest release of the monthly GRACE level-2 (L2) product (RL06), expressed  
263 as dimensionless spherical harmonic coefficients up to degree and order 90, are down-  
264 loaded for the period of April 2002 to December 2012 from the Center for Space Re-  
265 search (CSR, <http://www2.csr.utexas.edu/grace/RL06.html>). A limited length  
266 of the GRACE data is used here since the global hydrological model outputs of  
267 *Schellekens et al. (2017)* were available until 2012.

268 Recommended corrections are applied to generate monthly TWS fields from the  
269 GRACE product, i.e., degree 1 coefficients are replaced by those from *Swenson et al.*  
270 (2008) to account for the movement of the Earth’s center of mass. The zonal degree  
271 2 spherical harmonic coefficients (C20) are replaced by more stable ones derived from  
272 Satellite Laser Ranging (SLR) data (*Chen et al., 2007*). Surface deformations known  
273 as the Glacial Isostatic Adjustment (GIA) are reduced using the output of the model  
274 provided by *Wahr and Zhong (2012)*. GRACE level-2’s correlated errors are reduced  
275 by applying the DDK2 an-isotropic de-correlation filter (*Kusche et al., 2009*). The  
276 application of smoothing filters causes a spatial leakage problem, which is evaluated  
277 in terms of TWS errors following the approach in *Wahr et al. (1998)*; *Khaki et al.*  
278 (2018c) over the world’s 33 largest river basins as shown in Fig. ESM.1. An overview  
279 of the TWS’s strength and our error estimates is shown in ESM-section 2 (see Figure  
280 ESM.2).

### 281 *2.2. Global Hydrological Model (GHM) Outputs*

282 Monthly water balance components from six large-scale Global Hydrological Mod-  
283 els (GHMs) including PCR-GLOBWB (*Van Beek et al., 2011*; *Wada et al., 2014*),  
284 SURFEX-TRIP (*Decharme et al., 2013*), LISFLOOD (*Van Der Knijff et al., 2010*),  
285 HBV-SIMREG (*Lindström et al., 1997*), W3RA (*Van Dijk, 2010*), and ORCHIDEE  
286 (*Polcher et al., 2011*) are used in this study to provide a priori information about  
287 groundwater, soil moisture, surface water, canopy, and snow water storage com-  
288 ponents. The output of these models are published by the earth2Observe Tier-1  
289 (*Schellekens et al., 2017*), and are available at 0.5° spatial resolution covering the pe-  
290 riod of 1979–2012 which can be downloaded from <http://earth2observe.github.io/water-resource-reanalysis-v1>.

292 Although, these models are structurally different, i.e., they use different method-  
293 ology to simulate water changes, they are driven by the same reanalysis-based forcing  
294 data set, WFDEI (WATCH Forcing Data methodology applied to ERA-Interim re-  
295 analysis *Weedon et al., 2014*). In other words, all hydrological models that are used

296 in this study may represent the TWS, but their respective approaches for simulating  
297 TWS and its corresponding storage compartments are not identical. For example,  
298 *Schellekens et al. (2017)* state that PCR-GLOBWB and SURFEX-TRIP contain all  
299 surface and sub-surface water storage components in their TWS estimation. In con-  
300 trast, TWS derived from LISFLOOD, HBV-SIMREG, and W3RA are equal to the  
301 summation of groundwater, soil moisture, and snow, while that of ORCHIDEE is  
302 the summation of soil moisture, surface water, and snow storage components.

303 An overview of the model outputs used in this study is provided in Table 1, and  
304 the linear trend (as a representative of monotonic long-term storage changes) fitted  
305 to the model outputs are shown in [ESM-section 3](#).

TABLE 1

306 To ensure that the TWS estimates from GRACE L2 data and model outputs have  
307 the same spectral content,  $0.5^\circ$  resolution hydrological model outputs are transformed  
308 into the spectral domain and truncated to the maximum degree and order 90. The  
309 conversion follows an ordinary integration while considering the Gibbs effect along  
310 the coast lines (for more details please see, e.g., *Wang et al., 2006; Forootan et al.,*  
311 *2013*). Basin averages of each model components and their errors in terms of water  
312 storage are obtained from the same procedure used to process GRACE L2 data, i.e.,  
313 implemented here following *Wahr et al. (1998); Khaki et al. (2018c)*.

### 314 *2.3. El Niño Southern Oscillation (ENSO) Index*

315 The El Niño Southern Oscillation (ENSO, *Barnston and Livezey, 1987*) is a  
316 large-scale inter-annual climate variability phenomenon in the Tropical Pacific Ocean,  
317 which affects the climate of many regions of the Earth due to its ability to change  
318 the global atmospheric circulation, which influences temperature and precipitation  
319 across the globe (*Trenberth, 1990; Forootan et al., 2016*). The positive phase on  
320 ENSO is known as El Niño, and its opposite phase is known as La Nina. The  
321 ENSO index used in this study is derived from sea surface temperature in the Niño  
322 3.4 region ( $5^\circ N - 5^\circ S, 170^\circ E - 120^\circ W$ ). Monthly ENSO index (Niño 3.4 index),  
323 which is provided by the NOAA National Center for Environmental Information  
324 (NCEI) covering 1948 onward, is downloaded from [https://www.esrl.noaa.gov/](https://www.esrl.noaa.gov/psd/data/correlation/nina34.data)  
325 [psd/data/correlation/nina34.data](https://www.esrl.noaa.gov/psd/data/correlation/nina34.data). This index will be used later in this study  
326 to demonstrate whether the DMDA-derived surface and sub-surface water storage  
327 estimates are closer to the reality than those from individual models.

### 328 *2.4. Satellite Altimetry of Major Lakes*

329 Water level measurement by satellite altimetry has been developed and optimised  
330 for open oceans, yet improved post-processing techniques can be used to obtain reli-

331 able satellite altimetry-derived height measurements within inland water bodies such  
 332 as lakes, rivers, floodplains and wetlands (e.g., *Moore and Williams, 2014; Uebbing*  
 333 *et al., 2015*). In this study, satellite altimetry-derived surface water observations  
 334 are used to validate TWS changes of GRACE and models as well as surface wa-  
 335 ter derived from GHMs and the DMDA method. Satellite altimetry time series of  
 336 major global lakes are available from the U.S. Department of Agriculture (USDA)  
 337 (<https://ipad.fas.usda.gov/>). Repeated observations of the TOPEX/Poseidon  
 338 (T/P), Jason-1, and Jason2/OSTM altimetry missions are included in this database.  
 339 USDA provides time series of lake water level variations from 1992 to the present-day  
 340 within 81 lakes, and from 2008 to present-day within more than 280 lakes around  
 341 the world. An assessment over 14 lakes located within 8 river basins of this study  
 342 is presented in section 4.4 for the period of 2002–2012. Details of these lakes are  
 343 reported in Table 2.

TABLE 2

### 344 3. Dynamic Model Data Averaging (DMDA) Method

345 In this section, we present the mathematical formulation of Dynamic Model Data  
 346 Averaging (DMDA), which follows the method of Dynamic Model Averaging (DMA,  
 347 *Raftery et al., 2010*) but with some modifications to achieve a recursive update of  
 348 hydrological model outputs using GRACE TWS data (Fig. 1 summarises the DMDA  
 349 method). It will also be shown that the implementation of DMDA combines the  
 350 benefits of state-space merging techniques, such as Kalman Filtering (KF, *Evensen,*  
 351 *1994*) or Particle Filtering (PF, *Gordon et al., 1993*), Markov Chain (MC, *Metropolis*  
 352 *et al., 1953; Chan and Geyer, 1994; Kuczera and Parent, 1998*), and Bayesian Model  
 353 Averaging (BMA, *Hsu et al., 2009*). DMDA can be applied in data assimilation  
 354 applications that work with only one model, e.g., (*Giroto et al., 2016; Khaki et al.,*  
 355 *2017c,b; Schumacher et al., 2018*), as well as in handling multi-model outputs as in  
 356 *Van Dijk et al. (2014)*.

357 DMDA is formulated based on the representation of a state-space equation, which  
 358 dynamically relates the GRACE TWS estimates and hydrological model outputs as:

$$y_t = z_t \theta_t + \epsilon_t, \quad (1)$$

$$\theta_t = \theta_{t-1} + \delta_t, \quad (2)$$

359 Equation (1) is known as ‘observation equation’ and represents a linear regression  
 360 between the observation  $y_t$  (GRACE TWS estimates) and the vector of predictors

361  $z_t$  (model-derived water storage simulations). The unknown regression parameter  
362  $\theta_t$ , commonly known as the ‘state vector’ ([Bernstein, 2005](#)), is allowed to evolve in  
363 time, according to equation (2), and is known as the ‘state equation’. In equations  
364 (1) and (2),  $\epsilon_t$  and  $\delta_t$  can be interpreted as the residual of output vector and state  
365 parameters, respectively. They are usually defined using a normal distribution with  
366 the mean value of zero and a standard deviation, which will be computed during the  
367 DMDA procedure.

368 It is worth mentioning here that the EnKF ([Evensen, 1994](#)) and PF are among  
369 popular algorithms that can be used to recursively update an estimate of the model  
370 states and produce corresponding innovation values given a sequence of observations  
371 in the state-space equation (similar to what introduced above). In theory, EnKF  
372 accomplishes this goal by linear projections, and the estimations in PF are performed  
373 through a Sequential Monte Carlo sampling. Comparing EnKF and PF, the latter  
374 includes a random element so it converges to the true posterior probability function  
375 if the number of samples is very large. While the strength of PF is in its ability to  
376 account for both Gaussian and non-Gaussian error distributions, it suffers from the  
377 curse of dimensionality, which means that the sample size increases exponentially  
378 with the dimension of the state-space in order to achieve a certain performance.  
379 This fact precludes the use of PF in high-dimensional data-model fusion problems  
380 ([Bengtsson et al., 2008](#); [Daum and Huang, 2003](#); [Snyder et al., 2008](#)). For linear and  
381 Gaussian-type state-space models, as presented in this study, the PF method will  
382 yield the same likelihood as EnKF when the number of simulations is large enough  
383 (this has been tested but the results are not shown to keep the focus of this study on  
384 presenting the DMDA). Therefore, the DMDA, which combines the benefits of the  
385 EnKF and it is mathematically rigorous like PF, is adopted for the global data-model  
386 integration of this study.

387 Equations (1) and (2) are formulated with the main assumption that there is little  
388 physical knowledge about how the defined regression model and its parameters are  
389 likely to evolve in time. However, we will show that, by introducing two parameters  
390 of  $\lambda$  and  $\alpha$ , which are referred to as ‘forgetting factors’, one can control the temporal  
391 dependency of the DMDA solutions. These two parameters provide the opportunity  
392 to treat model simulations and observations of each step temporally dependent on,  
393 or independent from, previous steps. Since changes in water storage depend on the  
394 history of hydrological processes, accounting for temporal dependency between water  
395 states sounds logical.

396 **Formulating DMDA to Update Multi-Model Outputs using GRACE TWS**

397 Here the DMDA method is formulated to update the outputs of multi-hydrological  
 398 models,  $M_k$ , (for six models:  $k = 1, \dots, 6$ ). It is worth mentioning that since available  
 399 models have different storage definitions, the length of the state vector can change  
 400 from one model to another. Additionally, the structure of each individual storage  
 401 components can also be defined differently in different models (e.g., the number of soil  
 402 layers does not remain constant in different hydrological models). These differences  
 403 can be handled by DMDA.

404 In the following,  $Y_t = [y_1, \dots, y_t]$  represents the vector of observations (i.e., GRACE  
 405 TWS estimates in our study) up to the time step  $t$ . To use this vector to update the  
 406 water storage simulation of a single-model, one can estimate the unknown (linear)  
 407 regression parameters ( $\theta_t$ ) as

$$\theta_{t-1}|Y_{t-1} \sim N(\hat{\theta}_{t-1}, \hat{\Sigma}_{t-1}). \quad (3)$$

408 The distribution of each parameter can be assumed to be normal with unknown  
 409 mean  $\hat{\theta}_{t-1}$  and the variance  $\hat{\Sigma}_{t-1}$ . The regression coefficients at time  $t$  ( $\theta_t$ ) can then  
 410 be obtained using  $\theta_{t-1}$  from equation (3) and by introducing  $\delta_t \sim \mathcal{N}(0, W_t)$  to the  
 411 state equation (equation (2)). Therefore, the desired parameters at time  $t$  are defined  
 412 by

$$\theta_t|Y_{t-1} \sim N(\hat{\theta}_{t-1}, R_t), \quad (4)$$

413 where

$$R_t = \hat{\Sigma}_{t-1} + W_t. \quad (5)$$

414 In equation (5),  $W_t$  is the covariance matrix of the state innovation vector ( $\delta_t$   
 415 in equation (2)) and it shows the dependency of the regression parameters at each  
 416 time point to the previous time. However, in practice, there is no information about  
 417 the temporal relationship between GRACE TWS estimates and hydrological model  
 418 outputs to be used to define  $W_t$ . Therefore, to mathematically define a temporal  
 419 dependency,  $R_t$  in equation (4) can be replaced by

$$R_t = \lambda^{-1} \hat{\Sigma}_{t-1}, \quad (6)$$

420 where  $\lambda$  ( $0 < \lambda \leq 1$ ) controls the influence of previous observations on the regression  
 421 value at time  $t$ , and is known as ‘forgetting factor’ in the DMDA method (see, e.g.,  
 422 *Fagin, 1964; Jazwinski, 2007*).

423 *Hannan et al. (1989)* indicated that in the recursive estimation of auto-regressive  
 424 models, the covariance of previous steps is derived as a weighted product of the

425 current step (i.e., weighted by  $\lambda^{-1}$  in equation (6)). By this assumption, the effective  
 426 window size of temporal dependency is estimated by  $1/(1 - \lambda)$ . In our case, we  
 427 choose  $\lambda$  to be 0.95, which means that for monthly data, the effective window size is  
 428 equivalent to 18 months. This value is chosen experimentally because it minimized  
 429 the Root Mean Square (RMS) of differences between TWS derived from DMDA and  
 430 GRACE.

431 To apply DMDA and update water storage simulated by  $K$  different models, the  
 432 parameter prediction of equation (4) is extended as

$$\theta_t^{(k)} | M_t = k, Y_{t-1} \sim N(\hat{\theta}_{t-1}^{(k)}, \lambda^{-1} \hat{\Sigma}_{t-1}^{(k)}), \quad k = 1, \dots, K, \quad (7)$$

433 where  $M_t = k$  denotes which model (from the  $k = 1, 2, \dots, K$  available models)  
 434 applies at time  $t$ , and the solution  $\theta_t^{(k)}$  and  $\hat{\Sigma}_{t-1}^{(k)}$  can be obtained using a Kalman  
 435 Filter (KF)-type update conditional on  $M_t = k$  for each sample. This (KF-type)  
 436 update at time  $t$  is derived as

$$\theta_t^{(k)} | Y_t \sim N(\hat{\theta}_t^{(k)}, \hat{\Sigma}_t^{(k)}). \quad (8)$$

437 Regression parameters to update multi-model storage simulations can be estimated  
 438 as

$$\hat{\theta}_t^{(k)} = \hat{\theta}_{t-1}^{(k)} + R_t^{(k)} z_t^{(k)} (V_t + z_t^{(k)} (R_t^{(k)} + Q_t^{(k)}) z_t^{(k)T})^{-1} (y_t^{(k)} - z_t^{(k)} \hat{\theta}_{t-1}^{(k)}), \quad (9)$$

439 where  $V_t$  is the covariance matrix of GRACE TWS estimates (our observation), and  
 440  $Q_t$  is the covariance matrix of predictor  $z_t$  (see equation (1)). In this study, the  
 441 leakage errors of model-derived TWS are estimated for the world's 33 river basins  
 442 (similar to those of GRACE). These errors are used to generate  $Q_t$ , which is therefore  
 443 a diagonal matrix in the DMDA implementation of this study. For a grid based  
 444 implementation of DMDA, one can use the full covariance matrix of GRACE TWS  
 445 similar to [Schumacher et al. \(2016\)](#). The covariance matrix  $\hat{\Sigma}_t$  in equation (8) can  
 446 be estimated from

$$\hat{\Sigma}_t^{(k)} = R_t^{(k)} - R_t^{(k)} z_t^{(k)T} (V_t + z_t^{(k)} (R_t^{(k)} + Q_t^{(k)}) z_t^{(k)T})^{-1} z_t^{(k)} R_t^{(k)}. \quad (10)$$

447 It is evident from equations (9) and (10) that the estimation of regression parame-  
 448 ter  $\hat{\theta}_t$  is conditional on a particular model. Therefore, the DMDA solution to obtain  
 449 unconditional results and update multi-model simulations involves calculating the  
 450 posterior model probability  $P(M_t = k | Y_t)$  as a weight for each model, which changes  
 451 at each time step. In the following, we show that time-variable weights need to be  
 452 computed for each model  $k$  by choosing a forgetting factor  $\alpha$  in a recursive method,

453 where  $k = 1, \dots, K$ . These weights are then used to average the models, which leads  
 454 to the best fit to the GRACE TWS estimates. This justifies the term ‘Dynamic’ in  
 455 the DMDA and makes the method different from other averaging techniques such as  
 456 the Bayesian Model Averaging (BMA).

457 Let us assume that  $P(M_t = k|Y_t) = \pi_{t|t,k}$ , then the posterior model probability  
 458 for each model  $k$  at time  $t$  can be estimated as

$$\pi_{t|t,k} = \frac{\pi_{t|t-1,k}P(y_t|M_t = k, Y_{t-1})}{\sum_{l=1}^K \pi_{t|t-1,l}P(y_t|M_t = l, Y_{t-1})}, \quad (11)$$

459 where,  $P(y_t|M_t = k, Y_{t-1})$  is the density of the observation at time  $t$ , conditional on  
 460 model  $k$ , as well as  $Y_{t-1} = [y_1, y_2, \dots, y_{t-1}]$ , which is estimated by a normal distribution  
 461 as

$$y_t|M_t = k, Y_{t-1} \sim N(z_t^{(k)}\hat{\theta}_{t-1}^{(k)}, V_t + z_t^{(k)}(R_t^{(k)} + Q_t^{(k)})z_t^{(k)T}), \quad (12)$$

462 and,  $\pi_{t|t-1,k}$  is the model prediction equation, which is defined by

$$\pi_{t|t-1,k} = \sum_{l=1}^K \pi_{t-1|t-1,k} a_{kl}. \quad (13)$$

463 In equation (12),  $\hat{\theta}_{t-1}^{(k)}$  is estimated using the KF-type update as formulated in  
 464 equations (9) and (10), while  $R_t^{(k)}$  is obtained from equation (6) by choosing a for-  
 465 getting factor  $\lambda$ , i.e., between 0 and 1.

466 In equation (13)  $a_{kl} = P(M_t = l|M_{t-1} = k)$  is the element of the  $K \times K$  transition  
 467 matrix  $A(a_{kl})$  between models, which can be onerous when the number of models is  
 468 large, e.g., for  $K$  models and  $\tau$  time steps, the number of combinations of models will  
 469 be  $K^{2\tau}$ . In our study, we have 6 hydrological models, and 122 time steps over the  
 470 entire period of the study (2002–2012), which leads to  $6^{244}$  combinations of models.  
 471 To specify the transition matrix  $A$ , one way is to use the Markov Chain Monte Carlo  
 472 method (MCMC, [Geyer, 2011](#)), which will typically be computationally expensive.  
 473 Therefore, in this study, we avoid the implicit specification of the transition matrix  
 474 using the forgetting factor of  $0 < \alpha < 1$ , which has the same role as  $\lambda$  in equation  
 475 (6). As a result, the model prediction equation (13) can be rewritten as

$$\pi_{t|t-1,k} = \frac{\pi_{t-1|t-1,k}^\alpha}{\sum_{l=1}^K \pi_{t-1|t-1,l}^\alpha}. \quad (14)$$

476 The posterior model probability, or weights, for each model at time  $t$  is estimated  
 477 in a recursive solution between equations (11), (12), and (14). This process is initial-  
 478 ized by setting  $\pi_{0|0,k} = \frac{1}{K}$  for  $k = 1, \dots, K$ , and assigning a prior values to the initial

479 condition of the states  $\theta_0^{(k)} \sim N(0, \Sigma_0^{(k)})$  and  $\Sigma_0^{(k)} = \text{Variance}(y_t^{(k)}) / \text{Variance}(z_t^{(k)})$ .  
 480 The reason of choosing this prior value is that in a linear regression, a regression  
 481 coefficient for a predictor  $z_t$  is likely to be less than the standard deviation of the ob-  
 482 servations  $y_t$  divided by the standard deviation of predictors  $z_t$  (for more information  
 483 see e.g., [Raftery, 1993](#)). In our numerical evaluation of DMDA with six hydrological  
 484 models, the optimum regression estimates are found when  $0.85 < \alpha < 0.9$ , because  
 485 the RMS of differences between the DMDA-derived TWS and those of GRACE were  
 486 at a minimum here. By choosing a forgetting factor  $\alpha = 0.9$ , we assume a tem-  
 487 poral smoothing window with 36 month time steps between 6 hydrological model  
 488 ensembles to predict posterior probability values of each model  $k$  at time  $t$ . It means  
 489 that the contribution of hydrological models at time  $t - 37$  in to the posterior model  
 490 probability of each model  $k$  at time  $t$  is negligible. The length of this smoothing  
 491 window is reduced e.g., to 8 months if we choose  $\alpha = 0.2$ .

492 The multi-model predictions of  $y_t$  is a weighted average of model specific pre-  
 493 diction  $\hat{y}_t$ , using the posterior model probabilities,  $\pi_{t|t,k} = Pr(M_t = k|Y_t)$ , as its  
 494 weights, i.e.,

$$\hat{y}_t^{DMDA} = \sum_{l=1}^K \pi_{t|t,l} \hat{y}_t^{(l)}, \quad (15)$$

495 where  $\hat{y}_t^{(k)} = z_t^{(k)} \hat{\theta}_t^{(k)}$ .

496 The posterior model probability for each model at time  $t$ , along with the estimated  
 497 time-variable regression parameter  $\theta_t^{(k)}$  from KF-type updating equation (9) are used  
 498 to estimate the multi-model prediction of water storage components as

$$\hat{z}_{j,t}^{DMDA} = \sum_{l=1}^K \pi_{t|t,l} z_{j,t}^{(l)} \hat{\theta}_{j,t}^{(l)}, \quad (16)$$

499 where  $j$  represents each of the water storage components, i.e. groundwater, soil  
 500 moisture, surface water, canopy, and snow. To update the water storage simulations  
 501 of a single-model using the GRACE TWS estimates and the DMDA approach,  $K$   
 502 needs to be set to 1, and the prediction step is limited to the conditional estimation  
 503 of the parameter  $\theta_t^{(k)} | M_t^{(k)}$  using equation (9).

504 The posterior model probability can also be used to estimate unconditional prob-  
 505 ability distribution of regression parameters  $\Theta_t = (\theta_t^{(1)}, \dots, \theta_t^{(K)})$  given by observation  
 506  $Y_t$  following

$$p(\Theta_t | Y_t) = \sum_{l=1}^K p(\theta_t^{(l)} | M_t = l, Y_t) P(M_t = l | Y_t), \quad (17)$$

507 where  $p(\theta_t^{(k)}|M_t^{(k)}, Y_t)$  shows the conditional distribution of  $\theta_t^{(k)}$  which is approxi-  
 508 mated by a normal distribution as:

$$\theta_t^{(k)}|M_t^{(k)}, Y_t \sim N(\hat{\theta}_t^{(k)}, \hat{\Sigma}_t^{(k)}). \quad (18)$$

509 The DMDA approach can be recovered to a standard Bayesian Model Averaging  
 510 (BMA, [Hoeting et al. \(1999\)](#)) when  $\alpha = \lambda = 1$ . Then the posterior model probability  
 511 of model  $k$  is given by

$$P(M_t = k|Y_t) = \frac{p(Y_t|M_t = k)}{\sum_{l=1}^K p(Y_t|M_t = l)}, \quad (19)$$

512 where  $p(Y_t|M_t = k)$  is the marginal likelihood, obtained by integrating the product of  
 513 the likelihood,  $P(Y_t|\theta^{(k)}, M_t = k)$ , and the prior,  $P(\theta^{(k)}|M_t = k)$ , over the parameter  
 514 space (see also [Hsu et al., 2009](#)). Figure 1 summarises the work-flow of the DMDA  
 515 approach.

FIGURE 1

## 516 4. Results

### 517 4.1. Setup a Simulation to Test the Performance of DMDA

518 Before applying the DMDA method on real data, its performance is tested in a  
 519 controlled synthetic simulation, where the results of the Bayesian update are known  
 520 by definition. In the first step of our simulation, we aim to compare DMDA and BMA  
 521 in terms of updating hydrological model outputs with respect to the observations (i.e.,  
 522 GRACE TWS estimates in this study). In the second step, it will be shown that the  
 523 DMDA-derived time-variable weights are the same as the expected values.

524 To make the synthetic study simple, we assumed that TWS is defined as the  
 525 summation of just groundwater and soil moisture components. By this definition,  
 526 the time series of groundwater and soil moisture of two hydrological models, i.e., here  
 527 selected as LISFLOOD ( $M_1$ ) and SURFEX-TRIP ( $M_2$ ), are introduced as predictors  
 528 to the DMDA, and TWS derived from a third model, here selected to be PCR-  
 529 GLOBWB, is considered as the observation (here standing in for GRACE derived  
 530 TWS). By this choice, after applying DMDA to merge  $M_1$  and  $M_2$  with simulated  
 531 observed TWS, we expect that the updated (DMDA-derived) groundwater and soil  
 532 moisture storage estimates will be fitted to those of simulated observation. Here, we  
 533 selected results within the Niger River Basin (id:20 in Fig. [ESM.1](#)), covering the pe-  
 534 riod of 2002–2012. Figure 2 (A) shows the PCR-GLOBWB TWS as our observation,

535 Fig. 2 (B) represents the time series of groundwater and soil moisture derived from  
536  $M_1$  (B1, B3, blue curves) and  $M_2$  (B2, B4, green curves), while the expected value  
537 of DMDA-derived groundwater and soil moisture (simulated observation) are shown  
538 with the red color curves in these figures.

539 The magnitude of minimum (Min), maximum (Max) and the Root Mean Square  
540 (RMS) of the signal for all simulated data sets can be found in Table 3. The uncer-  
541 tainty of these data sets are computed following a least squares error propagation,  
542 while considering the leakage error of GRACE TWS in the Niger River Basin. It  
543 is worth mentioning that the final results of the simulation do not depend on the  
544 selection of models and the adopted simplification. The RMS of differences between  
545 the simulated TWS and two selected models (reported in Table 3) indicates that  $M_2$   
546 (RMS of  $\Delta_{TWS} = 14.1$  mm) had a better agreement with the observations compared  
547 to  $M_1$  (RMS of  $\Delta_{TWS} = 18.6$  mm). Figure 2 (C1) shows the estimated weights for  
548 the first model ( $W_1$ , Mean= 0.47) and second model ( $W_2$ , Mean= 0.53) obtained  
549 using DMDA (equation (11)). These results show that the model which had a better  
550 agreement with observations gained higher weights.

551 To compare DMDA and BMA methods to average hydrological components, we  
552 apply both of these methods on simulated data sets. The final results are shown in  
553 Fig. 2 (D1: groundwater) and (D2: soil moisture). Groundwater, soil moisture, and  
554 consequently TWS derived from DMDA shows better agreement with the expected  
555 values in comparison to the BMA results. The RMS of errors for both methods are  
556 reported in Table 3, which indicates that although TWS derived from BMA follow  
557 the expected value (RMS of error= 8.4 mm), the obtained individual components  
558 from this method are not close to the simulated values (RMS of errors of 20.4 mm and  
559 18.6 mm are found for groundwater and soil moisture, respectively). A considerable  
560 decrease in the differences between hydrological components and the expected values  
561 of DMDA shows that the method is suitable to update multi-model water storage  
562 estimates. Details of the numerical comparisons can be found in Table 3.

563 In the second step of our simulation, we use the weights of the first step ( $W_1$ ,  $W_2$ ,  
564 Fig. 2 (C1)) plus a temporal white noise with standard deviation of 0.02 m (equal  
565 to the standard deviation of GRACE TWS error within the Niger River Basin)  
566 to simulate GRACE like TWS estimates. Reconstructed weights after applying the  
567 DMDA for the second time, using the new synthetic TWS observations, are shown in  
568 Fig. 2 (C2). The correlation coefficient between  $W_1$  and  $W_2$  with their reconstructed  
569 values is found to be 0.73 and the RMS of the reconstruction's errors is found to be  
570 0.18. This indicates that the DMDA-derived weights are close to reality and further  
571 motivates us to apply it on real data sets.

FIGURE 2

TABLE 3

572

573 *4.2. DMDA Weights to Compare Global Hydrological Models*

574 TWS derived from DMDA is a weighted average of selected models by estimating  
575 time varying weights based on the Bayes rule as in equation (15). Figure 3 shows the  
576 estimated weights for ten basins with the largest RMS of differences between TWS  
577 derived from individual models and GRACE TWS. Time-variable weights derived  
578 from DMDA allow us (1) to quantify the quality and compare individual water stor-  
579 age simulations derived from each global hydrological model against GRACE TWS  
580 for different periods of time, and (2) to separate GRACE TWS in a Bayesian frame-  
581 work, while considering different model structures and errors within and between  
582 model simulations and GRACE data. The average of weights during 2002–2012 is  
583 considered as the basis to select the best model in DMDA results over 33 river basins  
584 which is shown in the middle of Fig. 3. From our numerical results, PCR-GLOBWB  
585 is found to gain the largest weights during this period, thus, it contributed the most  
586 in the DMDA-derived TWS in North Asia, Central Africa, and North America.  
587 The weights computed for SURFEX-TRIP are found to be larger than other models  
588 within the snow-dominated regions, such as, the Yukon and Mackenzie in the north  
589 part of America and the Lena in the Northeast Asia. Our results confirm the inves-  
590 tigation by *Schellekens et al. (2017)*, who compared the mentioned models against  
591 the Interactive Multi-sensor snow and Ice Mapping System (IMS, *Ramsay, 1998*).  
592 Apparently, multiple snow layers of SURFEX-TRIP helps it to better simulate snow  
593 dynamics during the cold seasons.

594 We also find that SURFEX-TRIP received the highest averaged weights (com-  
595 pared to other models) within the Amazon and Brahmaputra River Basins during  
596 2002–2012. The explanation is that SURFEX-TRIP likely better accounts for (1)  
597 the snow coverage of the Brahmaputra River Basin, (2) the considerable contribution  
598 of surface water storage components in the TWS changes within the Amazon River  
599 Basin, and (3) the overall dry period within both basins (*Chen et al., 2009; Khandu*  
600 *et al., 2016*), specially the extreme hydrological droughts of 2005 and 2010 (*Forootan*  
601 *et al., 2019*). In the Amazon River Basin, we also find the highest performance for  
602 SURFEX-TRIP between 2009-2011. *Chen et al. (2009)* reported that in 2009 the  
603 Amazon River Basin experienced an extreme flood, which increased the magnitude  
604 of inter-annual TWS in this basin. TWS changes within the Amazon are also closely  
605 connected to the ENSO events in the tropical Pacific (*Kousky et al., 1984; Ropelewski*

606 *and Halpert, 1987*). Later we will show that surface water derived from SURFEX-  
607 TRIP shows the highest correlation with ENSO index in comparison with the other  
608 models of this study. This could be another reason that we derive the highest weights  
609 for SURFEX-TRIP between 2009-2011 within the Amazon River Basin.

610 Our results (Fig. 3) indicate that within the river basins with considerable irriga-  
611 tion (such as the Indus, Euphrates, and Orange River Basins), the relatively highest  
612 weights are assigned to the LISFLOOD and ORCHIDEE, where both account for  
613 human water-use (*Schellekens et al., 2017*). ORCHIDEE is also found to perform  
614 well within the Brahmaputra, Ganges, and Murray River Basins, each of which expe-  
615 rienced a strong decline in rainfall over the entire period of our study (e.g.,  $9.0 \pm 4.0$   
616 mm/decade between 1994–2014 over Ganges and Brahmaputra *Khandu et al., 2016*).  
617 Specifically, ORCHIDEE contains 14 soil layers (see Table 1) that help it to better  
618 resolve vertical water exchange within the irrigated regions. In *ESM-section 2*, it is  
619 shown that GRACE TWS changes within the Murray River Basin are considerably  
620 influenced by ENSO events (see also *Forootan et al., 2012, 2016*), and the simulated  
621 outputs of ORCHIDEE reflects these changes better than the other tested models  
622 justifying the higher weights that are assigned to this model within the DMDA pro-  
623 cedure. In *ESM-section 5*, we show that after applying the DMDA, model-derived  
624 TWS simulations are tuned to GRACE TWS.

### FIGURE 3

#### 625 4.3. DMDA-Derived Individual Water Storage Estimates

626 The estimated weights for the six models of section 4.2 along with the computed  
627 regression coefficients  $\hat{\theta}_t$  (see the flowchart of Fig. 1), are used to compute the  
628 DMDA-derived groundwater, soil moisture, and surface water. In order to interpret  
629 the monotonic changes of water storage changes within the river basins, a long-term  
630 linear trend is fitted to the DMDA results that are shown in Figure 4, and the  
631 numerical values are reported in Table 4.

### FIGURE 4

632

### TABLE 4

633 Figure 4 (a1) and (a2) show the linear trend fitted to the DMDA-derived ground-  
634 water and its uncertainty. The results indicate a decrease in groundwater in 42% of  
635 the assessed river basis (i.e., 14 of 33). The largest decreasing trends are found in  
636 basins with large-scale irrigation such as the Ganges ( $-14.77 \pm 0.25$  mm/yr), Indus  
637 ( $-8.26 \pm 0.16$  mm/yr) and Euphrates ( $-5.36 \pm 0.23$  mm/yr). The results confirm

638 the findings by *Khandu et al. (2016)*, *Forootan et al. (2019)*, and *Voss et al. (2013)*,  
639 respectively. The strongest increasing trends in groundwater are seen in the To-  
640 cantins basin (South America) at the rate of  $2.41 \pm 0.47$  mm/yr, the Okavango  
641 (South Africa) with a rate of  $1.74 \pm 1.31$  mm/yr, and the Lena (Northeast Asia)  
642 with  $1.74 \pm 0.11$  mm/yr. However, all of these trends are not statistically significant.  
643 The positive trends in groundwater storage in these last two basins are associated  
644 to the heavy rainfalls, seasonal floods and the geographical location of the Okavango  
645 Delta (*McCarthy et al., 1998*), and underground ice melting caused by global warm-  
646 ing (*Dzhamalov et al., 2012*), respectively. Comparisons between the DMDA-derived  
647 groundwater and those of hydrological models indicate that after merging GRACE  
648 TWS with output from multiple hydrological models, the linear trend has changed  
649 considerably. This means that introducing GRACE data can successfully modify the  
650 anthropogenic effects, which are not well simulated by models (linear trends of the  
651 modelled groundwater are shown in [ESM-section 3](#)).

652 The linear trend fitted to the DMDA-derived soil moisture and its uncertainty  
653 are shown in Fig. 4 (b1) and (b2). We find strongest increasing trends in soil  
654 moisture estimates within the Murray (Australia), Okavango, and Orinoco (South  
655 America) River Basins with rates of  $6.66 \pm 0.15$ ,  $3.92 \pm 0.55$ , and  $3.45 \pm 0.26$  mm/yr  
656 respectively, and largest decreasing trends in the Brahmaputra and Euphrates with  
657 rates of  $-7.00 \pm 0.69$  and  $-5.75 \pm 0.39$  mm/yr.

658 Figure 4 (c1) and (c2) show the linear trends and their uncertainty fitted to  
659 the surface water storage estimated through the DMDA method. Linear trends of  
660 surface water within the 28 out of the 33 river basins are found to be statistically  
661 insignificant (values between -1 and +1 mm/yr). The strongest negative trends are  
662 found in the Euphrates, Murray, and Okavango River Basins with rates of  $-2.09 \pm$   
663  $0.09$ ,  $-1.47 \pm 0.04$ , and  $-1.42 \pm 0.37$  mm/yr respectively. In contrast, the largest  
664 positive trends are found within the Amazon and Colorado, at the rate of  $1.43 \pm$   
665  $0.06$  and  $1.04 \pm 0.04$  mm/yr, respectively. The heavy flood during the summer of  
666 2008–2009 (*Marengo et al., 2011*; *Chen et al., 2010*), which was considerably bigger  
667 than the temporal mean, likely caused these positive trend in the Amazon River  
668 Basin. Negative trends in all three water storage compartments of the Euphrates  
669 River Basin (groundwater  $-5.36 \pm 0.23$  mm/yr, soil moisture  $-5.75 \pm 0.39$  mm/yr,  
670 and surface water  $-2.09 \pm 0.09$  mm/yr) can be associated to both irrigation and  
671 long-term drought as shown by *Forootan et al. (2017)*.

#### 672 4.3.1. Contribution of ENSO in DMDA-Derived Water Storage Components

673 To demonstrate that the DMDA-derived surface and sub-surface water storage  
674 estimates are closer to the reality than those from any individual model, we extract

675 the dominant ENSO mode from the DMDA estimates and compare them with climate  
676 indices (see e.g., [Anyah et al., 2018](#)) in terms of temporal correlation coefficients with  
677 the ENSO index (-Niño 3.4 index, Fig. 5, 6, and 7). The reason for this comparison  
678 is that GRACE captures considerable variability due to the ENSO events ([Phillips  
679 et al., 2012](#); [Forootan et al., 2018](#)). Therefore, by merging multi-model outputs with  
680 GRACE data, their skill in representing water storage changes due to large-scale  
681 teleconnections would be improved.

682 In order to extract the ENSO modes from the DMDA-derived water storage  
683 estimates and the original outputs of the six models (PCRGLOB-WB, SURFEX-  
684 TRIP, LISFLOOD, HBV-SIMREG, W3RA, and ORCHIDEE) Principal Component  
685 Analysis (PCA, [Lorenz, 1956](#)) method is applied after removing the long-term linear  
686 trend and seasonality from hydrological components. More details about PCA results  
687 and extracting ENSO modes from DMDA water storage components are reported in  
688 [ESM-section 6](#).

689 Figure 5 shows temporal correlations between the ENSO mode of groundwater  
690 (from DMDA and original models) and the ENSO index. Maximum and minimum  
691 correlation of 0.75 and 0.53 corresponding to a maximum lag of up to 2 months are  
692 found globally between the DMDA groundwater and the ENSO index, respectively.  
693 Smaller correlations are found between the original models and the ENSO index.  
694 Among these models, W3RA and HBV-SIMREG indicate stronger correlations ( $\sim$   
695 0.6 and  $\sim$  0.4 respectively) with the ENSO index with a maximum lag of 2 months.  
696 Other models such as LISFLOOD and SURFEX-TRIP indicate notably different  
697 correlations (compared to HBV-SIMREG and W3RA as well as that of DMDA)  
698 with ENSO in various basins. We find small positive correlations with a maximum  
699 value of 0.3 between original PCR-GLOBWB's groundwater and the ENSO index.  
700 Although the maximum lag of 3 month is estimated in most of the 33 basins, a lag  
701 of 15 months is estimated for the Nile, Okavango, and Zambezi (Africa), Colorado  
702 and Nelson (North America), Ob, Lena, and Yellow (Asia) River Basins, which are  
703 likely not realistic (see, e.g., [Awange et al., 2014](#); [Anyah et al., 2018](#)).

## FIGURE 5

704 Similar assessments are performed between the soil moisture and surface water  
705 storage changes with the ENSO index and the results are shown in Figs. 6 and  
706 7. Correlation coefficients of up to 0.8 are computed from the DMDA estimates  
707 with a maximum lag of up to 2 months. Among the six models, correlation in  
708 soil moisture of the SURFEX-TRIP and LISFLOOD models is found to be the  
709 highest, i.e., correlations of 0.6 to 0.8 within the 33 river basins examined here.  
710 PCR-GLOBWB and W3RA show a correlation of  $\sim$  0.5, while those from HBV-

711 SIMREG and ORCHIDEE are different from our other estimations, for example,  
712 less than 0.1 in the Niger and Nile River Basins, and greater than 0.75 in North  
713 Asia. *Khaki et al. (2018b)* indicate that over the Nile River Basin, all the three  
714 hydrological components, (i.e., groundwater, surface water, and soil moisture) are  
715 strongly influenced by ENSO. Therefore, the obtained correlation of 0.1 in the Nile  
716 River Basin from HBV-SIMREG is likely not realistic.

#### FIGURE 6

717 The DMDA-derived surface water storage is compared with those of PCR-GLOBWB,  
718 SURFEX-TRIP, and ORCHIDEE, which contain the surface water storage compart-  
719 ment. The correlation coefficients are found to be generally smaller than those of soil  
720 moisture and groundwater components (with a maximum of 0.5), which likely shows  
721 that the modelling of surface water needs improvement because in reality surface wa-  
722 ter in lakes and rivers within regions like East Africa shows an immediate response to  
723 ENSO (e.g., *Becker et al., 2010; Khaki et al., 2018b*). Figure 7 shows that the surface  
724 water storage output of SURFEX-TRIP had the highest correlations with the ENSO  
725 index in all basins of America (values between 0.33 and 0.51) and Africa (values  
726 between 0.23 and 0.48), while ORCHIDEE shows the highest correlations (values  
727 between 0.32 and 0.58) in most parts of Asia. The correlations for PCR-GLOBWB  
728 are found to be relatively smaller, i.e., between 0.1 and 0.2 with lags of between 5-12  
729 months. Comparisons between the DMDA and original model outputs indicate that  
730 combining models with GRACE data improve the correlations with the ENSO index  
731 and the correlation lags are considerably reduced globally. It is worth mentioning  
732 that the DMDA results that are presented here are derived by setting the  $\alpha$  value  
733 in equation (14) to 0.9. This means that we assume a 36 month temporal correla-  
734 tions between water storage simulations of the six models. This value guarantee an  
735 extraction of the ENSO modes within two PCA modes after merging GRACE and  
736 model outputs.

#### FIGURE 7

#### 737 4.4. *Evaluating the DMDA Results with satellite altimetry observation*

738 To validate our results, TWS and surface water derived from DMDA and six  
739 hydrological models are compared with independent surface water observations from  
740 satellite altimetry. The results are shown for various regions with reliable satellite  
741 altimetry measurements such as the Nile, Niger, and Zambezi River Basins in Africa,  
742 Ob and Euphrates in Asia, St' Lawrence and Nelson in North America, and Orinoco  
743 in South Africa. Here, we assessed 14 lakes located in the 8 mentioned river basins.

744 Comparisons are performed in terms of correlation coefficients between TWS and  
745 surface water estimates (within the river basins), and water mass variations within  
746 the lakes (i.e., lake level heights from satellite altimetry data are converted to mass  
747 variations following *Moore and Williams (2014)*). The numerical results are sum-  
748 marized in Table 5, which indicates that after implementing the DMDA method,  
749 correlation coefficients are increased in most of the lakes. High values are found in  
750 the Nile River Basin, e.g., Tana Lake (0.718), Euphrates (Tharthar Lake, 0.569), and  
751 Niger (Chad Lake, 0.558), while low values are found in the Kainiji Lake of the Niger  
752 River Basin (0.102) and Winnipegosis of the Nelson River Basins (0.249). It should  
753 be noted here that although low correlations are found for some lakes, the values are  
754 increased when compared with the original model simulations. More details can be  
755 found in [ESM-section 7](#).

TABLE 5

## 756 5. Summary and Conclusion

757 In this study, the method of Dynamic Model Data Averaging (DMDA) is intro-  
758 duced, which can be used (1) to compare multi-model (individual) water storage  
759 simulations with GRACE-derived Terrestrial Water Storage (TWS) estimates; and  
760 (2) to separate GRACE TWS into horological water storage compartments. DMDA  
761 combines the property of Kalman Filter (equations (9), (10)) and a Bayesian weight-  
762 ing (equation (11)) to fit multi-model water storage changes to GRACE TWS esti-  
763 mates. The method is flexible in accounting for errors in observations and a priori  
764 information (equation 9 and equation 10), and can deal with state vectors of different  
765 length.

766 The benefit of the DMDA method over the commonly used PF or PS methods  
767 are twofold: 1) these methods might not be efficient for high-dimensional fusion  
768 tasks (e.g., *Snyder et al., 2008*; *Van Leeuwen, 2009*) such as the global hydrological  
769 application presented here, but the DMDA’s computational load is lower than these  
770 techniques; 2) DMDA provides time-variable weights that can be used to under-  
771 stand the behavior of a priori information (here the output of hydrological models)  
772 against GRACE TWS estimates, while considering their errors. The advantage of  
773 the DMDA over the Ensemble Kalman Filter-based of techniques is that the poste-  
774 rior distributions are computed through a Bayesian rule that result in more reliable  
775 estimations of states and their errors, while avoiding the high computational loads  
776 of the PF techniques.

777 A realistic synthetic example was defined to evaluate the performance of DMDA  
778 (Fig. 2), which showed that the method is able to correctly separate GRACE TWS

779 estimates into its individual hydrological components. We also showed that the  
780 DMDA’s estimation of temporal weights (for each model) was close to the real-  
781 ity, and can be used to assess the performance of available models. Based on the  
782 real data, we showed that the representation of linear trends and seasonality within  
783 global hydrological models, as well as their water storage changes due to the El Niño  
784 Southern Oscillation (ENSO) can be improved using DMDA, while considering the  
785 uncertainties of models and observations (see Fig. 1). Our results also showed that  
786 how the DMDA method is able to deal with models with different structures, and  
787 how it updates their water storage simulations while considering their errors. Consid-  
788 ering these arguments, we believe that the new water storage estimates, i.e., models  
789 combined with GRACE, are of great values and can be used for further hydrological  
790 and climate research investigations compared to model or GRACE only estimates.  
791 Therefore, the presented results can be considered as one step forward to improve  
792 model deficiencies following the insights of *Scanlon et al. (2018)*. In what follows,  
793 the main conclusions and remarks of this study are summarized.

- 794 • Estimated weights (Fig. 3) showed that the PCR-GLOBWB model gained the  
795 largest weights, thus, it contributed the most in the DMDA-derived TWS in  
796 North Asia, North America, and the center of Africa. SURFEX-TRIP per-  
797 formed best within basins with dominant surface water storage changes, as  
798 well as in snow-dominant regions. The LISFLOOD and ORCHIDEE models  
799 were found to perform well within irrigated basins, and those affected by ENSO  
800 events.
- 801 • DMDA results in Fig. 4 (a1) showed that considerable trends exist in ground-  
802 water storage changes within the Ganges, Indus, and Euphrates basins during  
803 2002–2012. These changes are dominantly influenced by anthropogenic modi-  
804 fications. Trends in soil moisture (Fig. 4 (b1)) were found to be mostly related  
805 to meteorological prolonged drought events such as those in the Brahmaputra  
806 and Euphrates River Basins.
- 807 • DMDA was able to modify the ENSO mode of water storage variability in  
808 most of the world’s 33 largest river basins (see Fig. 5, Fig. 6, and Fig. 7).  
809 DMDA assigned the biggest corrections of ENSO mode in groundwater to the  
810 Nile, Murray, Tocantins, Ob, Okavango and Orange River Basins. The highest  
811 corrections of the ENSO mode in soil moisture were found for the Nile, Niger,  
812 Zambezi, and Amur River Basins, and in surface water to Nile, Niger, Congo,  
813 Tocantins, and Murray River Basin. For example, the correlation coefficient  
814 between groundwater storage and ENSO in the Murray River Basin changed

815 from -0.2 to 0.6. For the Nile River Basin, they changed from 0.1 to 0.4 for soil  
816 moisture, and from 0.3 to 0.7 for the surface water compartment.

- 817 • Comparison between TWS and surface water derived from DMDA with inde-  
818 pendent surface water observations from satellite altimetry (Fig. [ESM.15](#) and  
819 Fig. [ESM.16](#) in [ESM-section 7](#)) showed that, DMDA was able to correctly de-  
820 tect the best performing model and maximize its contribution in the dynamic  
821 averaging process which enhanced the reality of water storage estimates.
- 822 • To implement the DMDA in this study a forgetting factor of 0.95 was con-  
823 sidered in equation (6), which is equivalent to the temporal dependency in  
824 estimating time variable regression parameters in equation (2). In section 3,  
825 it was shown that this selection is equivalent to 18 months temporal depen-  
826 dency between GRACE TWS observations and model simulations. This value  
827 is selected because the DMDA results were closest to that of GRACE. After  
828 selecting this value, we also obtained a distinguishable ENSO mode from the  
829 DMDA-derived TWS and individual water storage estimates. Therefore, we  
830 conclude that this temporal lag might be considered in other works that at-  
831 tempt to apply sequential mergers or smoothers to assimilate observed water  
832 storage data into models.
- 833 • In order to reduce the computational load of this work, instead of implementing  
834 a Markov Chain Monte Carlo (MCMC) technique to estimate the transition  
835 matrix between models in equation (13), a forgetting factor of 0.9 was con-  
836 sidered in equations (14). This might be replaced with an efficient MCMC  
837 implementation in future.

838 The DMDA method, introduced in this study, has the potential to be used in dif-  
839 ferent climate and hydrological applications to compare available models (which can  
840 be of various types of hydrological or climate models) against reliable observations.  
841 It can also be used to generate ensembles from multi-model outputs such as climate  
842 projections. The application of this study can also be extended by incorporating  
843 other types of remote sensing observations such as satellite based soil moisture or  
844 water level data beside those of GRACE. A secondary application of the DMDA  
845 can also be devoted to its application for predicting (or extrapolating) water storage  
846 estimates. To achieve this purpose, however, the DMDA's formulation needs to be  
847 extended. For example, one approach can be to use the DMDA weights, which are  
848 computed for the period of study, to identify best models in different river basins cov-  
849 ering different seasons. By analysing this information and knowing the TWS in the

850 future, one can use a combination of different model runs (weighted by the DMDA  
851 outputs) and extrapolate the surface and sub-surface water storage estimates.

852 **References**

- 853 Anyah, R. O., E. Forootan, J. L. Awange, and M. Khaki (2018), Understanding  
854 linkages between global climate indices and terrestrial water storage changes over  
855 africa using grace products, *Science of The Total Environment*, 635, 1405–1416,  
856 doi:10.1016/j.scitotenv.2018.04.159.
- 857 Awange, J. L., E. Forootan, M. Kuhn, J. Kusche, and B. Heck (2014), Water stor-  
858 age changes and climate variability within the Nile basin between 2002 and 2011,  
859 *Advances in Water Resources*, 73, 1–15, doi:10.1016/j.advwatres.2014.06.010.
- 860 Bai, P., X. Liu, and C. Liu (2018), Improving hydrological simulations by incor-  
861 porating grace data for model calibration, *Journal of Hydrology*, 557, 291–304,  
862 doi:10.1016/j.jhydrol.2017.12.025.
- 863 Bain, A., and D. Crisan (2008), *Fundamentals of stochastic filtering*, vol. 60, Springer  
864 Science & Business Media, doi:10.1007/978-0-387-76896-0.
- 865 Banerjee, S., B. P. Carlin, and A. E. Gelfand (2004), *Hierarchical modeling and*  
866 *analysis for spatial data*, Chapman and Hall/CRC.
- 867 Barnston, A. G., and R. E. Livezey (1987), Classification, seasonality and persistence  
868 of low-frequency atmospheric circulation patterns, *Monthly weather review*, 115(6),  
869 1083–1126, doi:10.1175/1520-0493(1987)115(1083:CSAPOL)2.0.CO;2.
- 870 Becker, M., W. Llovel, A. Cazenave, A. Güntner, and J.-F. Crétaux (2010), Recent  
871 hydrological behavior of the east African great lakes region inferred from grace,  
872 satellite altimetry and rainfall observations, *Comptes Rendus Geoscience*, 342(3),  
873 223–233, doi:10.1016/j.crte.2009.12.010.
- 874 Bengtsson, T., P. Bickel, B. Li, et al. (2008), Curse-of-dimensionality revisited: Col-  
875 lapse of the particle filter in very large scale systems, in *Probability and statistics:*  
876 *Essays in honor of David A. Freedman*, pp. 316–334, Institute of Mathematical  
877 Statistics, doi:10.1214/193940307000000518.
- 878 Bernstein, D. S. (2005), *Matrix mathematics: Theory, facts, and formulas with ap-*  
879 *plication to linear systems theory*, vol. 41, Princeton university press Princeton.
- 880 Boening, C., J. K. Willis, F. W. Landerer, R. S. Nerem, and J. Fasullo (2012), The  
881 2011 la niña: So strong, the oceans fell, *Geophysical Research Letters*, 39(19),  
882 doi:10.1029/2012GL053055.

- 883 Chan, K. S., and C. J. Geyer (1994), Discussion: Markov chains for explor-  
884 ing posterior distributions, *The Annals of Statistics*, 22(4), 1747–1758, doi:  
885 10.1214/aos/1176325754.
- 886 Chen, J. L., C. R. Wilson, J. S. Famiglietti, and M. Rodell (2007), Attenuation effect  
887 on seasonal basin-scale water storage changes from grace time-variable gravity,  
888 *Journal of Geodesy*, 81(4), 237–245, doi:10.1007/s00190-006-0104-2.
- 889 Chen, J. L., C. R. Wilson, B. D. Tapley, Z. L. Yang, and G. Y. Niu (2009), 2005  
890 drought event in the amazon river basin as measured by grace and estimated  
891 by climate models, *Journal of Geophysical Research: Solid Earth*, 114(B5), doi:  
892 10.1029/2008JB006056.
- 893 Chen, J. L., C. R. Wilson, and B. D. Tapley (2010), The 2009 exceptional amazon  
894 flood and interannual terrestrial water storage change observed by grace, *Water*  
895 *Resources Research*, 46(12), doi:10.1029/2010WR009383.
- 896 Daum, F., and J. Huang (2003), Curse of dimensionality and particle filters, in *2003*  
897 *IEEE Aerospace Conference Proceedings (Cat. No. 03TH8652)*, vol. 4, pp. 4\_1979–  
898 4\_1993, IEEE, doi:10.1109/AERO.2003.1235126.
- 899 Decharme, B., E. Martin, and S. Faroux (2013), Reconciling soil thermal and hydro-  
900 logical lower boundary conditions in land surface models, *Journal of Geophysical*  
901 *Research: Atmospheres*, 118(14), 7819–7834, doi:10.1002/jgrd.50631.
- 902 Del Moral, P., and L. Miclo (2000), Branching and interacting particle systems ap-  
903 proximations of feynman-kac formulae with applications to non-linear filtering, in  
904 *Seminaire de probabilites XXXIV*, pp. 1–145, Springer, doi:10.1007/BFb0103798.
- 905 Döll, P., F. Kaspar, and B. Lehner (2003), A global hydrological model for deriving  
906 water availability indicators: model tuning and validation, *Journal of Hydrology*,  
907 270(1-2), 105–134, doi:10.1016/S0022-1694(02)00283-4.
- 908 Duan, Q., N. K. Ajami, X. Gao, and S. Sorooshian (2007), Multi-model ensemble hy-  
909 drologic prediction using bayesian model averaging, *Advances in Water Resources*,  
910 30(5), 1371–1386, doi:10.1016/j.advwatres.2006.11.014.
- 911 Dzhamalov, R. G., G. N. Krichevets, and T. I. Safronova (2012), Current changes in  
912 water resources in lena river basin, *Water Resources*, 39(2), 147–160, doi:10.1134/  
913 S0097807812020042.

- 914 Evensen, G. (1994), Sequential data assimilation with a nonlinear quasi-geostrophic  
915 model using monte carlo methods to forecast error statistics, *Journal of Geophys-*  
916 *ical Research: Oceans*, 99(C5), 10,143–10,162, doi:10.1029/94JC00572.
- 917 Evensen, G. (2003), The ensemble kalman filter: Theoretical formulation  
918 and practical implementation, *Ocean dynamics*, 53(4), 343–367, doi:10.1007/  
919 s10236-003-0036-9.
- 920 Fagin, S. L. (1964), Recursive linear regression theory, optimal filter theory, and error  
921 analysis of optimal systems, in *IEEE international convention record*, vol. 12, pp.  
922 216–245.
- 923 Fang, H., N. Tian, Y. Wang, M. Zhou, and M. A. Haile (2018), Nonlinear bayesian  
924 estimation: from kalman filtering to a broader horizon, *IEEE/CAA Journal of*  
925 *Automatica Sinica*, 5(2), 401–417, doi:10.1109/JAS.2017.7510808.
- 926 Feng, W., M. Zhong, J. M. Lemoine, R. Biancale, H.-T. Hsu, and J. Xia (2013),  
927 Evaluation of groundwater depletion in north china using the gravity recovery  
928 and climate experiment (grace) data and ground-based measurements, *Water Re-*  
929 *sources Research*, 49(4), 2110–2118, doi:10.1002/wrcr.20192.
- 930 Forootan, E., and J. Kusche (2012), Separation of global time-variable gravity signals  
931 into maximally independent components, *Journal of Geodesy*, 86(7), 477–497, doi:  
932 0.1007/s00190-011-0532-5.
- 933 Forootan, E., and J. Kusche (2013), Separation of deterministic signals using inde-  
934 pendent component analysis (ica), *Studia Geophysica et Geodaetica*, 57(1), 17–26,  
935 doi:10.1007/s11200-012-0718-1.
- 936 Forootan, E., J. Awange, J. Kusche, B. Heck, and A. Eicker (2012), Independent  
937 patterns of water mass anomalies over australia from satellite data and models,  
938 *Remote sensing of environment*, 124, 427–443, doi:10.1016/j.rse.2012.05.023.
- 939 Forootan, E., O. Didova, J. Kusche, and A. Löcher (2013), Comparisons of atmo-  
940 spheric data and reduction methods for the analysis of satellite gravimetry ob-  
941 servations, *Journal of Geophysical Research: Solid Earth*, 118(5), 2382–2396, doi:  
942 10.1002/jgrb.50160.
- 943 Forootan, E., R. Rietbroek, J. Kusche, M. A. Sharifi, J. L. Awange, M. Schmidt,  
944 P. Omondi, and J. S. Famiglietti (2014), Separation of large scale water storage  
945 patterns over iran using grace, altimetry and hydrological data, *Remote Sensing*  
946 *of Environment*, 140, 580–595, doi:10.1016/j.rse.2013.09.025.

- 947 Forootan, E., J. L. Awange, M. Schumacher, R. O. Anyah, A. I. J. M. van Dijk,  
948 J. Kusche, et al. (2016), Quantifying the impacts of enso and iod on rain gauge  
949 and remotely sensed precipitation products over australia, *Remote sensing of En-*  
950 *vironment*, 172, 50–66, doi:10.1016/j.rse.2015.10.027.
- 951 Forootan, E., A. Safari, A. Mostafaie, M. Schumacher, M. Delavar, and J. L. Awange  
952 (2017), Large-scale total water storage and water flux changes over the arid and  
953 semiarid parts of the middle east from grace and reanalysis products, *Surveys in*  
954 *Geophysics*, 38(3), 591–615, doi:10.1007/s10712-016-9403-1.
- 955 Forootan, E., J. Kusche, M. Talpe, C. K. Shum, and M. Schmidt (2018), Develop-  
956 ing a complex independent component analysis (cica) technique to extract non-  
957 stationary patterns from geophysical time series, *Surveys in Geophysics*, 39(3),  
958 435–465, doi:10.1007/s10712-017-9451-1.
- 959 Forootan, E., M. Khaki, M. Schumacher, V. Wulfmeyer, N. Mehrnegar, A. I. J. M.  
960 van Dijk, L. Brocca, S. Farzaneh, F. Akinluyi, G. Ramillien, C. Shum, J. L.  
961 Awange, and A. Mostafaie (2019), Understanding the global hydrological droughts  
962 of 2003–2016 and their relationships with teleconnections, *Science of The Total*  
963 *Environment*, 650, 2587–2604, doi:10.1016/j.scitotenv.2018.09.231.
- 964 Frappart, F., and G. Ramillien (2018), Monitoring groundwater storage changes  
965 using the gravity recovery and climate experiment (grace) satellite mission: A  
966 review, *Remote Sensing*, 10(6), 829, doi:10.3390/rs10060829.
- 967 Geyer, C. J. (2011), Introduction to markov chain monte carlo, *Handbook of Markov*  
968 *Chain Monte Carlo*, p. 46.
- 969 Giroto, M., G. J. De Lannoy, R. H. Reichle, and M. Rodell (2016), Assimilation of  
970 gridded terrestrial water storage observations from grace into a land surface model,  
971 *Water Resources Research*, 52(5), 4164–4183, doi:10.1002/2015WR018417.
- 972 Giroto, M., G. J. De Lannoy, R. H. Reichle, M. Rodell, C. Draper, S. N. Bhanja,  
973 and A. Mukherjee (2017), Benefits and pitfalls of grace data assimilation: A case  
974 study of terrestrial water storage depletion in india, *Geophysical research letters*,  
975 44(9), 4107–4115, doi:10.1002/2017GL072994.
- 976 Gordon, N. J., D. J. Salmond, and A. F. Smith (1993), Novel approach to  
977 nonlinear/non-gaussian bayesian state estimation, in *IEE proceedings F (radar*  
978 *and signal processing)*, vol. 140, pp. 107–113, IET, doi:10.1049/ip-f-2.1993.0015.

- 979 Hanington, P., Q. T. To, P. D. T. Van, N. A. V. Doan, and A. S. Kiem (2017), A  
980 hydrological model for interprovincial water resource planning and management:  
981 a case study in the long xuyen quadrangle, mekong delta, vietnam, *Journal of*  
982 *Hydrology*, *547*, 1–9, doi:10.1016/j.jhydrol.2017.01.030.
- 983 Hannan, E. J., A. McDougall, and D. Poskitt (1989), Recursive estimation of au-  
984 toregressions, *Journal of the Royal Statistical Society. Series B (Methodological)*,  
985 *51*(2), 217–233, doi:10.1111/j.2517-6161.1989.tb01759.x.
- 986 Hoeting, J. A., D. Madigan, A. E. Raftery, and C. T. Volinsky (1999), Bayesian  
987 model averaging: A tutorial, *Statistical Science*, *14*(4), 382–417.
- 988 Hsu, K.-l., H. Moradkhani, and S. Sorooshian (2009), A sequential bayesian approach  
989 for hydrologic model selection and prediction, *Water Resources Research*, *45*(12),  
990 doi:10.1029/2008WR006824.
- 991 Hurkmans, R., P. A. Troch, R. Uijlenhoet, P. Torfs, and M. Durcik (2009), Effects  
992 of climate variability on water storage in the colorado river basin, *Journal of*  
993 *hydrometeorology*, *10*(5), 1257–1270, doi:10.1175/2009JHM1133.1.
- 994 Jazwinski, A. H. (2007), *Stochastic processes and filtering theory*, Courier Corpora-  
995 tion.
- 996 Khaki, M., B. Ait-El-Fquih, I. Hoteit, E. Forootan, J.L., and M. Kuhn (2017a), A  
997 two-update ensemble kalman filter for land hydrological data assimilation with an  
998 uncertain constraint, *Journal of Hydrology*, *555*, 447–462, doi:10.1016/j.jhydrol.  
999 2017.10.032.
- 1000 Khaki, M., I. Hoteit, M. Kuhn, J. L. Awange, E. Forootan, A. I. J. M. Van Dijk,  
1001 M. Schumacher, and C. Pattiaratchi (2017b), Assessing sequential data assimi-  
1002 lation techniques for integrating grace data into a hydrological model, *Advances in*  
1003 *Water Resources*, *107*, 301–316, doi:10.1016/j.advwatres.2017.07.001.
- 1004 Khaki, M., M. Schumacher, E. Forootan, M. Kuhn, J. L. Awange, and A. I. J. M.  
1005 van Dijk (2017c), Accounting for spatial correlation errors in the assimilation of  
1006 grace into hydrological models through localization, *Advances in Water Resources*,  
1007 *108*, 99–112, doi:10.1016/j.advwatres.2017.07.024.
- 1008 Khaki, M., B. Ait-El-Fquih, I. Hoteit, E. Forootan, J. L. Awange, and M. Kuhn  
1009 (2018a), Unsupervised ensemble kalman filtering with an uncertain constraint for  
1010 land hydrological data assimilation, *Journal of Hydrology*, *564*, 175–190, doi:10.  
1011 1016/j.jhydrol.2018.06.080.

- 1012 Khaki, M., J. L. Awange, E. Forootan, and M. Kuhn (2018b), Understanding the  
1013 association between climate variability and the Nile's water level fluctuations and  
1014 water storage changes during 1992–2016, *Science of The Total Environment*, *645*,  
1015 1509–1521, doi:10.1016/j.scitotenv.2018.07.212.
- 1016 Khaki, M., E. Forootan, M. Kuhn, J. L. Awange, L. Longuevergne, and Y. Wada  
1017 (2018c), Efficient basin scale filtering of GRACE satellite products, *Remote Sensing  
1018 of Environment*, *204*, 76–93, doi:10.1016/j.rse.2017.10.040.
- 1019 Khaki, M., E. Forootan, M. Kuhn, J. L. Awange, F. Papa, and C. K. Shum (2018d),  
1020 A study of Bangladesh's sub-surface water storages using satellite products and  
1021 data assimilation scheme, *Science of the Total Environment*, *625*, 963–977, doi:  
1022 10.1016/j.scitotenv.2017.12.289.
- 1023 Khaki, M., E. Forootan, M. Kuhn, J. L. Awange, A. I. J. M. van Dijk, M. Schu-  
1024 macher, and M. A. Sharifi (2018e), Determining water storage depletion within  
1025 Iran by assimilating GRACE data into the W3RA hydrological model, *Advances in  
1026 Water Resources*, *114*, 1–18, doi:10.1016/j.advwatres.2018.02.008.
- 1027 Khandu, K., E. Forootan, M. Schumacher, J. L. Awange, and H. Müller-Schmied  
1028 (2016), Exploring the influence of precipitation extremes and human water use on  
1029 total water storage (TWS) changes in the Ganges-Brahmaputra-Meghna river basin,  
1030 *Water Resources Research*, *52*(3), 2240–2258, doi:10.1002/2015WR018113.
- 1031 Kousky, V. E., M. T. Kagano, and I. F. Cavalcanti (1984), A review of the southern  
1032 oscillation: oceanic-atmospheric circulation changes and related rainfall anomalies,  
1033 *Tellus A*, *36*(5), 490–504, doi:10.1111/j.1600-0870.1984.tb00264.x.
- 1034 Kuczera, G., and E. Parent (1998), Monte Carlo assessment of parameter uncertainty  
1035 in conceptual catchment models: the Metropolis algorithm, *Journal of Hydrology*,  
1036 *211*(1-4), 69–85, doi:10.1016/S0022-1694(98)00198-X.
- 1037 Kusche, J., R. Schmidt, S. Petrovic, and R. Rietbroek (2009), Decorrelated GRACE  
1038 time-variable gravity solutions by GFZ, and their validation using a hydrological  
1039 model, *Journal of Geodesy*, *83*(10), 903–913, doi:10.1007/s00190-009-0308-3.
- 1040 Lindström, G., B. Johansson, M. Persson, M. Gardelin, and S. Bergström (1997),  
1041 Development and test of the distributed HBV-96 hydrological model, *Journal of  
1042 hydrology*, *201*(1-4), 272–288, doi:10.1016/S0022-1694(97)00041-3.

- 1043 Long, D., Y. Pan, J. Zhou, Y. Chen, X. Hou, Y. Hong, B. R. Scanlon, and L. Longuev-  
1044 ergne (2017), Global analysis of spatiotemporal variability in merged total water  
1045 storage changes using multiple grace products and global hydrological models,  
1046 *Remote sensing of environment*, *192*, 198–216, doi:10.1016/j.rse.2017.02.011.
- 1047 Lorenz, E. N. (1956), Empirical orthogonal functions and statistical weather predic-  
1048 tion.
- 1049 Marengo, J. A., C. A. Nobre, G. Sampaio, L. F. Salazar, and L. S. Borma (2011),  
1050 Climate change in the amazon basin: Tipping points, changes in extremes, and  
1051 impacts on natural and human systems, in *Tropical rainforest responses to climatic*  
1052 *change*, pp. 259–283, Springer, doi:10.1007/978-3-642-05383-2\_9.
- 1053 McCarthy, T. S., A. Bloem, and P. A. Larkin (1998), Observations on the hydrology  
1054 and geohydrology of the okavango delta, *South African Journal of Geology/Suid-*  
1055 *Afrikaanse Tydskrif vir Geologie*, *101*(2), 101–117.
- 1056 Metropolis, N., A. W. Rosenbluth, M. N. Rosenbluth, A. H. Teller, and E. Teller  
1057 (1953), Equation of state calculations by fast computing machines, *The journal of*  
1058 *chemical physics*, *21*(6), 1087–1092, doi:10.1063/1.1699114.
- 1059 Moore, P., and S. D. P. Williams (2014), Integration of altimetric lake levels and grace  
1060 gravimetry over africa: Inferences for terrestrial water storage change 2003–2011,  
1061 *Water Resources Research*, *50*(12), 9696–9720, doi:10.1002/2014WR015506.
- 1062 Mostafaie, A., E. Forootan, A. Safari, and M. Schumacher (2018), Comparing multi-  
1063 objective optimization techniques to calibrate a conceptual hydrological model  
1064 using in situ runoff and daily grace data, *Computational Geosciences*, *22*(3), 789–  
1065 814, doi:10.1007/s10596-018-9726-8.
- 1066 Ni, S., J. Chen, C. R. Wilson, J. Li, X. Hu, and R. Fu (2018), Global terrestrial water  
1067 storage changes and connections to enso events, *Surveys in Geophysics*, *39*(1), 1–  
1068 22, doi:10.1007/s10712-017-9421-7.
- 1069 Niu, G.-Y., Z.-L. Yang, K. E. Mitchell, F. Chen, M. B. Ek, M. Barlage, A. Kumar,  
1070 K. Manning, D. Niyogi, E. Rosero, et al. (2011), The community noah land sur-  
1071 face model with multiparameterization options (noah-mp): 1. model description  
1072 and evaluation with local-scale measurements, *Journal of Geophysical Research:*  
1073 *Atmospheres*, *116*(D12), doi:10.1029/2010JD015139.

- 1074 Phillips, T., R. Nerem, B. Fox-Kemper, J. Famiglietti, and B. Rajagopalan (2012),  
1075 The influence of enso on global terrestrial water storage using grace, *Geophysical*  
1076 *Research Letters*, *39*(16), doi:10.1029/2012GL052495.
- 1077 Plaza Guingla, D. A., R. De Keyser, G. J. De Lannoy, L. Giustarini, P. Matgen, and  
1078 V. R. Pauwels (2013), Improving particle filters in rainfall-runoff models: Appli-  
1079 cation of the resample-move step and the ensemble gaussian particle filter, *Water*  
1080 *Resources Research*, *49*(7), 4005–4021, doi:10.1002/wrcr.20291.
- 1081 Polcher, J., N. Bertrand, H. Biemans, D. B. Clark, M. Floerke, N. Gedney, D. Gerten,  
1082 T. Stacke, M. Van Vliet, and F. Voss (2011), Improvements in hydrological pro-  
1083 cesses in general hydrological models and land surface models within watch.
- 1084 Raftery, A. (1993), *Model selection and accounting for model uncertainty in linear*  
1085 *regression models*, Citeseer.
- 1086 Raftery, A. E., M. Kárný, and P. Ettlér (2010), Online prediction under model  
1087 uncertainty via dynamic model averaging: Application to a cold rolling mill, *Tech-*  
1088 *nometrics*, *52*(1), 52–66, doi:10.1198/TECH.2009.08104.
- 1089 Ramsay, B. H. (1998), The interactive multisensor snow and ice mapping system, *Hy-*  
1090 *drological Processes*, *12*(10-11), 1537–1546, doi:10.1002/(SICI)1099-1085(199808/  
1091 09)12:10/11<1537::AID-HYP679>3.0.CO;2-A.
- 1092 Rodell, M., P. R. Houser, U. Jambor, J. Gottschalck, K. Mitchell, C.-J. Meng, K. Ar-  
1093 senault, B. Cosgrove, J. Radakovich, M. Bosilovich, et al. (2004), The global land  
1094 data assimilation system, *Bulletin of the American Meteorological Society*, *85*(3),  
1095 381–394, doi:10.1175/BAMS-85-3-381.
- 1096 Rodell, M., I. Velicogna, and J. S. Famiglietti (2009), Satellite-based estimates of  
1097 groundwater depletion in india, *Nature*, *460*(7258), 999, doi:10.1038/nature08238.
- 1098 Ropelewski, C. F., and M. S. Halpert (1987), Global and regional scale precipitation  
1099 patterns associated with the el niño/southern oscillation, *Monthly weather review*,  
1100 *115*(8), 1606–1626, doi:10.1175/1520-0493(1987)115(1606:GARSPP)2.0.CO;2.
- 1101 Särkkä, S. (2013), *Bayesian filtering and smoothing*, vol. 3, Cambridge University  
1102 Press, doi:10.1201/b16018.
- 1103 Scanlon, B. R., Z. Zhang, H. Save, A. Y. Sun, H. M. Schmied, L. P. van Beek, D. N.  
1104 Wiese, Y. Wada, D. Long, R. C. Reedy, et al. (2018), Global models underestimate

- 1105 large decadal declining and rising water storage trends relative to grace satellite  
1106 data, *Proceedings of the National Academy of Sciences*, 115(6), E1080–E1089,  
1107 doi:10.1073/pnas.1704665115.
- 1108 Schellekens, J., E. Dutra, A. Martínez-de la Torre, G. Balsamo, A. van Dijk, F. S.  
1109 Weiland, M. Minvielle, J.-C. Calvet, B. Decharme, S. Eisner, et al. (2017), A global  
1110 water resources ensemble of hydrological models: the earth2observe tier-1 dataset,  
1111 *Earth System Science Data*, 9(2), 389–413, doi:10.5194/essd-9-389-2017.
- 1112 Schmeer, M., M. Schmidt, W. Bosch, and F. Seitz (2012), Separation of mass sig-  
1113 nals within grace monthly gravity field models by means of empirical orthogonal  
1114 functions, *Journal of Geodynamics*, 59, 124–132, doi:10.1016/j.jog.2012.03.001.
- 1115 Schumacher, M. (2016), Methods for assimilating remotely-sensed water storage  
1116 changes into hydrological models, Ph.D. thesis, Universitäts-und Landesbibliothek  
1117 Bonn.
- 1118 Schumacher, M., J. Kusche, and P. Döll (2016), A systematic impact assessment  
1119 of grace error correlation on data assimilation in hydrological models, *Journal of*  
1120 *Geodesy*, 90(6), 537–559, doi:10.1007/s00190-016-0892-y.
- 1121 Schumacher, M., E. Forootan, A. I. J. M. van Dijk, H. M. Schmied, R. S. Crosbie,  
1122 J. Kusche, and P. Döll (2018), Improving drought simulations within the murray-  
1123 darling basin by combined calibration/assimilation of grace data into the watgap  
1124 global hydrology model, *Remote Sensing of Environment*, 204, 212–228, doi:10.  
1125 1016/j.rse.2017.10.029.
- 1126 Sha, Z., J. Rougier, M. Schumacher, and J. Bamber (2018), Bayesian model-data  
1127 synthesis with an application to global glacio-isostatic adjustment, *Environmetrics*,  
1128 doi:10.1002/env.2530.
- 1129 Sheffield, J., E. F. Wood, and M. L. Roderick (2012), Little change in global drought  
1130 over the past 60 years, *Nature*, 491(7424), 435, doi:10.1038/nature11575.
- 1131 Singer, M. B., K. Michaelides, and D. E. Hobbey (2018), Storm 1.0: a simple,  
1132 flexible, and parsimonious stochastic rainfall generator for simulating climate  
1133 and climate change, *Geoscientific Model Development*, 11(9), 3713–3726, doi:  
1134 10.5194/gmd-11-3713-2018.
- 1135 Snyder, C., T. Bengtsson, P. Bickel, and J. Anderson (2008), Obstacles to high-  
1136 dimensional particle filtering, *Monthly Weather Review*, 136(12), 4629–4640, doi:  
1137 10.1175/2008MWR2529.1.

- 1138 Strassberg, G., B. R. Scanlon, and D. Chambers (2009), Evaluation of groundwa-  
1139 ter storage monitoring with the grace satellite: Case study of the high plains  
1140 aquifer, central united states, *Water Resources Research*, *45*(5), doi:10.1029/  
1141 2008WR006892.
- 1142 Swenson, S., D. Chambers, and J. Wahr (2008), Estimating geocenter variations from  
1143 a combination of grace and ocean model output, *Journal of Geophysical Research:*  
1144 *Solid Earth*, *113*(B8), doi:10.1029/2007JB005338.
- 1145 Tapley, B. D., S. Bettadpur, J. C. Ries, P. F. Thompson, and M. M. Watkins (2004),  
1146 Grace measurements of mass variability in the earth system, *Science*, *305*(5683),  
1147 503–505, doi:10.1126/science.1099192.
- 1148 Tian, S., P. Tregoning, L. J. Renzullo, A. I. J. M. van Dijk, J. P. Walker, V. R.  
1149 Pauwels, and S. Allgeyer (2017), Improved water balance component estimates  
1150 through joint assimilation of grace water storage and smos soil moisture retrievals,  
1151 *Water Resources Research*, *53*(3), 1820–1840, doi:10.1002/2016WR019641.
- 1152 Tiwari, V., J. Wahr, and S. Swenson (2009), Dwindling groundwater resources in  
1153 northern india, from satellite gravity observations, *Geophysical Research Letters*,  
1154 *36*(18), doi:10.1029/2009GL039401.
- 1155 Trenberth, K. E. (1990), Recent observed interdecadal climate changes in the north-  
1156 ern hemisphere, *Bulletin of the American Meteorological Society*, *71*(7), 988–993,  
1157 doi:10.1175/1520-0477(1990)071<0988:ROICCI>2.0.CO;2.
- 1158 Uebbing, B., J. Kusche, and E. Forootan (2015), Waveform retracking for improving  
1159 level estimations from topex/poseidon, jason-1, and jason-2 altimetry observations  
1160 over african lakes, *IEEE Transactions on Geoscience and Remote Sensing*, *53*(4),  
1161 2211–2224, doi:10.1109/TGRS.2014.2357893.
- 1162 Van Beek, L. P. H., Y. Wada, and M. F. P. Bierkens (2011), Global monthly water  
1163 stress: 1. water balance and water availability, *Water Resources Research*, *47*(7),  
1164 doi:10.1029/2010WR009791.
- 1165 Van Der Knijff, J. M., J. Younis, and A. P. J. De Roo (2010), Lisflood: a gis-  
1166 based distributed model for river basin scale water balance and flood simulation,  
1167 *International Journal of Geographical Information Science*, *24*(2), 189–212, doi:  
1168 10.1080/13658810802549154.

- 1169 Van Dijk, A. I. J. M. (2010), The australian water resources assessment system:  
1170 Technical 901 report 3, landscape model (version 0.5) technical description, csiro,  
1171 *Water for a Healthy Country National Research Flagship*.
- 1172 Van Dijk, A. I. J. M., L. J. Renzullo, Y. Wada, and P. Tregoning (2014), A global  
1173 water cycle reanalysis (2003–2012) merging satellite gravimetry and altimetry ob-  
1174 servations with a hydrological multi-model ensemble, *Hydrology and Earth System*  
1175 *Sciences*, 18(8), 2955–2973, doi:10.5194/hess-18-2955-2014.
- 1176 Van Leeuwen, P. J. (2009), Particle filtering in geophysical systems, *Monthly Weather*  
1177 *Review*, 137(12), 4089–4114, doi:10.1175/2009MWR2835.1.
- 1178 Voss, K. A., J. S. Famiglietti, M. Lo, C. De Linage, M. Rodell, and S. C. Swenson  
1179 (2013), Groundwater depletion in the middle east from grace with implications  
1180 for transboundary water management in the tigris-euphrates-western iran region,  
1181 *Water resources research*, 49(2), 904–914, doi:10.1002/wrcr.20078.
- 1182 Wada, Y., L. P. H. van Beek, F. C. S. Weiland, B. F. Chao, Y.-H. Wu, and M. F. P.  
1183 Bierkens (2012), Past and future contribution of global groundwater depletion to  
1184 sea-level rise, *Geophysical Research Letters*, 39(9), doi:10.1029/2012GL051230.
- 1185 Wada, Y., D. Wisser, and M. Bierkens (2014), Global modeling of withdrawal, al-  
1186 location and consumptive use of surface water and groundwater resources, *Earth*  
1187 *System Dynamics Discussions*, 5(1), 15–40, doi:10.5194/esdd-4-355-2013.
- 1188 Wahr, J., and S. Zhong (2012), Computations of the viscoelastic response of a 3-d  
1189 compressible earth to surface loading: an application to glacial isostatic adjustment  
1190 in antarctica and canada, *Geophysical Journal International*, 192(2), 557–572, doi:  
1191 10.1093/gji/ggs030.
- 1192 Wahr, J., M. Molenaar, and F. Bryan (1998), Time variability of the earth’s gravity  
1193 field: Hydrological and oceanic effects and their possible detection using grace,  
1194 *Journal of Geophysical Research: Solid Earth*, 103(B12), 30,205–30,229, doi:10.  
1195 1029/98JB02844.
- 1196 Wang, H., P. Wu, and Z. Wang (2006), An approach for spherical harmonic analysis  
1197 of non-smooth data, *Computers and geosciences*, 32(10), 1654–1668, doi:10.1016/  
1198 j.cageo.2006.03.004.
- 1199 Weedon, G. P., G. Balsamo, N. Bellouin, S. Gomes, M. J. Best, and P. Viterbo  
1200 (2014), The wfdei meteorological forcing data set: Watch forcing data methodology

- 1201 applied to era-interim reanalysis data, *Water Resources Research*, 50(9), 7505–  
1202 7514, doi:10.1002/2014WR015638.
- 1203 Weerts, A. H., and G. Y. El Serafy (2006), Particle filtering and ensemble kalman  
1204 filtering for state updating with hydrological conceptual rainfall-runoff models,  
1205 *Water resources research*, 42(9), doi:10.1029/2005WR004093.
- 1206 Werth, S., A. Güntner, S. Petrovic, and R. Schmidt (2009), Integration of grace  
1207 mass variations into a global hydrological model, *Earth Planet. Sci. Lett.*, 277(1),  
1208 166–173, doi:10.1016/j.epsl.2008.10.021.
- 1209 Zaitchik, B. F., M. Rodell, and R. H. Reichle (2008), Assimilation of grace terrestrial  
1210 water storage data into a land surface model: Results for the mississippi river basin,  
1211 *Journal of Hydrometeorology*, 9(3), 535–548, doi:10.1175/2007JHM951.1.
- 1212 Zhang, Z., B. Chao, J. Chen, and C. Wilson (2015), Terrestrial water storage anoma-  
1213 lies of yangtze river basin droughts observed by grace and connections with enso,  
1214 *Global and Planetary Change*, 126, 35–45, doi:10.1016/j.gloplacha.2015.01.002.



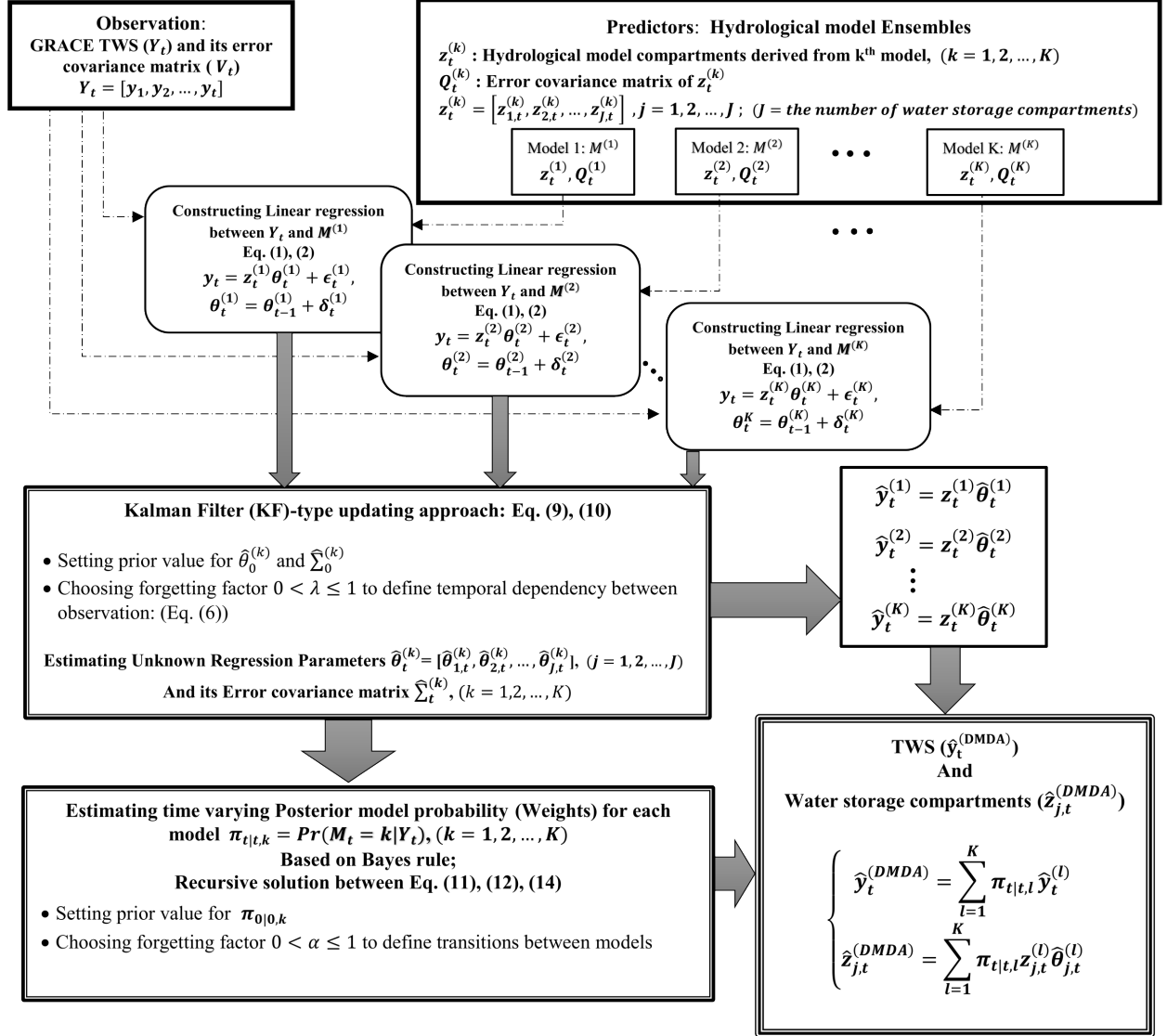


Figure 1: Flowchart of the Dynamic Model Data Averaging (DMDA) method. The framework can accept an arbitrary number of models and it can be extended to accept various type of observations.

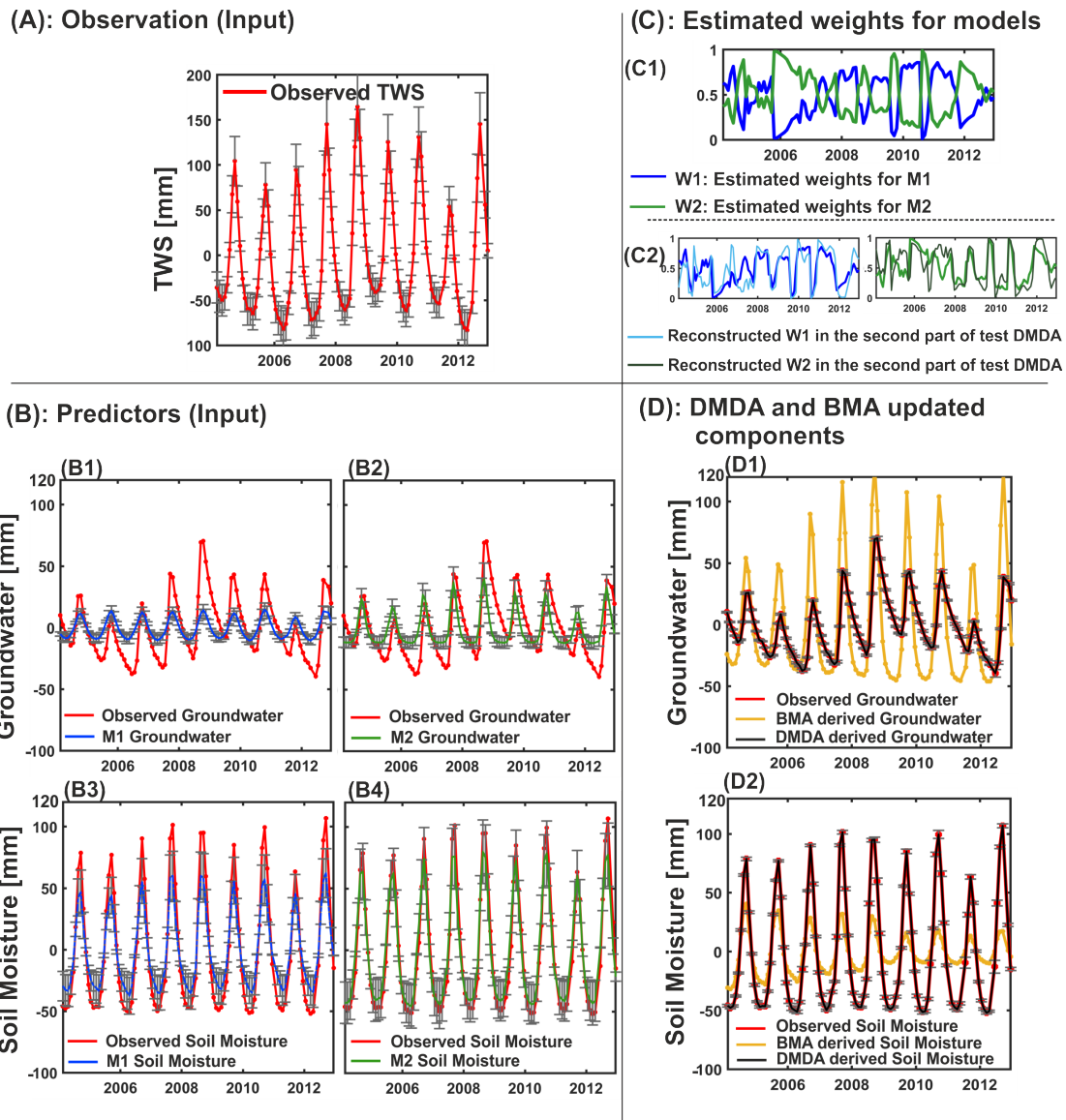


Figure 2: A synthetic example, where DMDA is applied in a controlled set up, to integrate 2 hydrological models (here selected as SURFEX-TRIP and LISFLOOD) with simulated observed TWS to separate its compartments (i.e., groundwater and soil moisture). All data sets in this simulation is related to the Niger River Basin and covering the period between 2002–2012; Figure 2 (A) shows TWS simulated from PCR-GLOBWB (here standing in for observed TWS); Figure 2 (B) shows the time series of groundwater and soil moisture derived from model 1 (B1, B3) and model 2 (B2, B4), which are considered as the input predictors in DMDA; Figure 2 (C1) presents the time varying weights estimated for two selected model, and Figure 2 (C2) shows the reconstructed of weights in the second step of our simulation. Figure 2 (D1) and (D2) show the updated hydrological components obtained from the DMDA and BMA method and comparison between the obtained results and the expected values derived form simulated observation data.

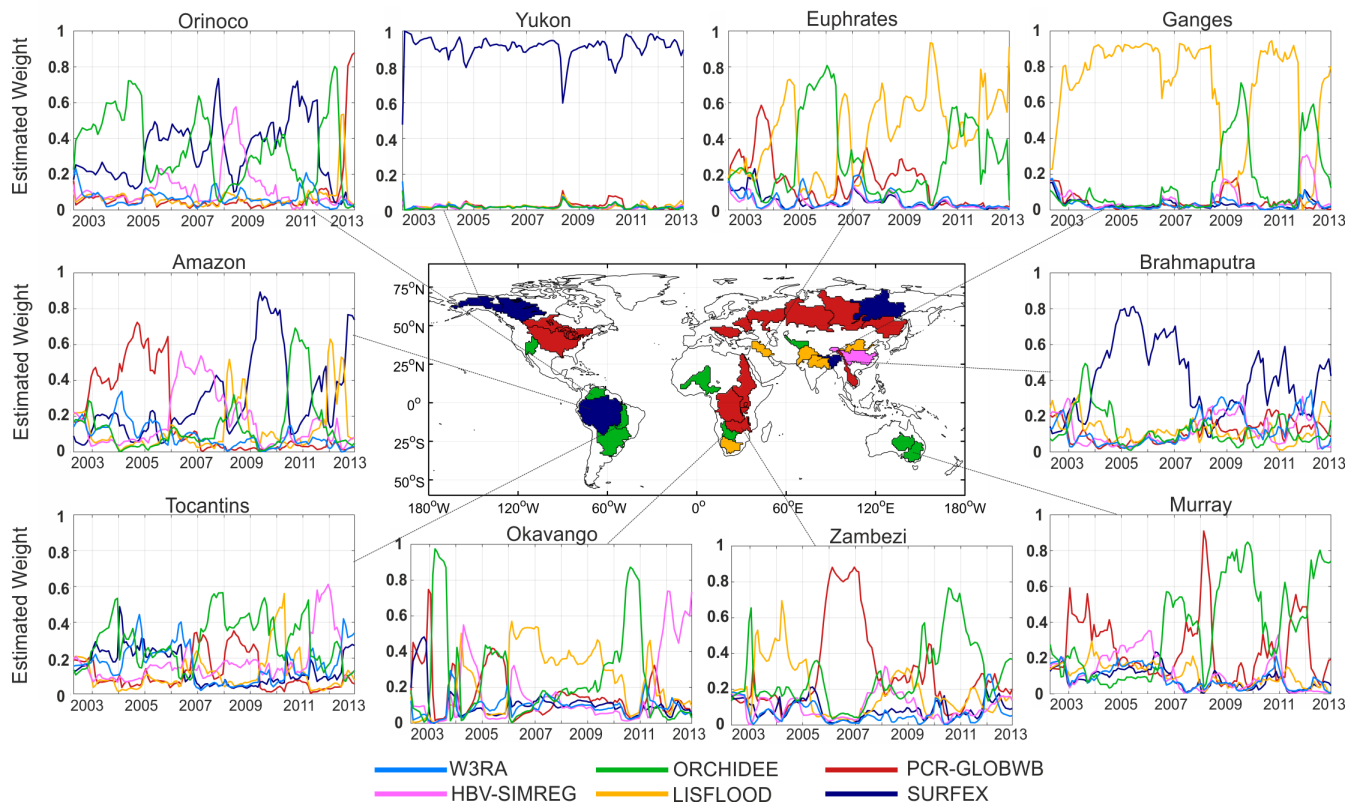


Figure 3: Posterior model probabilities for the six initially considered models, over 10 selected river basins with the biggest RMSEs computed using GRACE and models-derived TWS. In the middle of Fig 3 the most contributed models in the DMDA-derived TWS are shown over the world's 33 largest river basins, covering the period of 2002–2012.

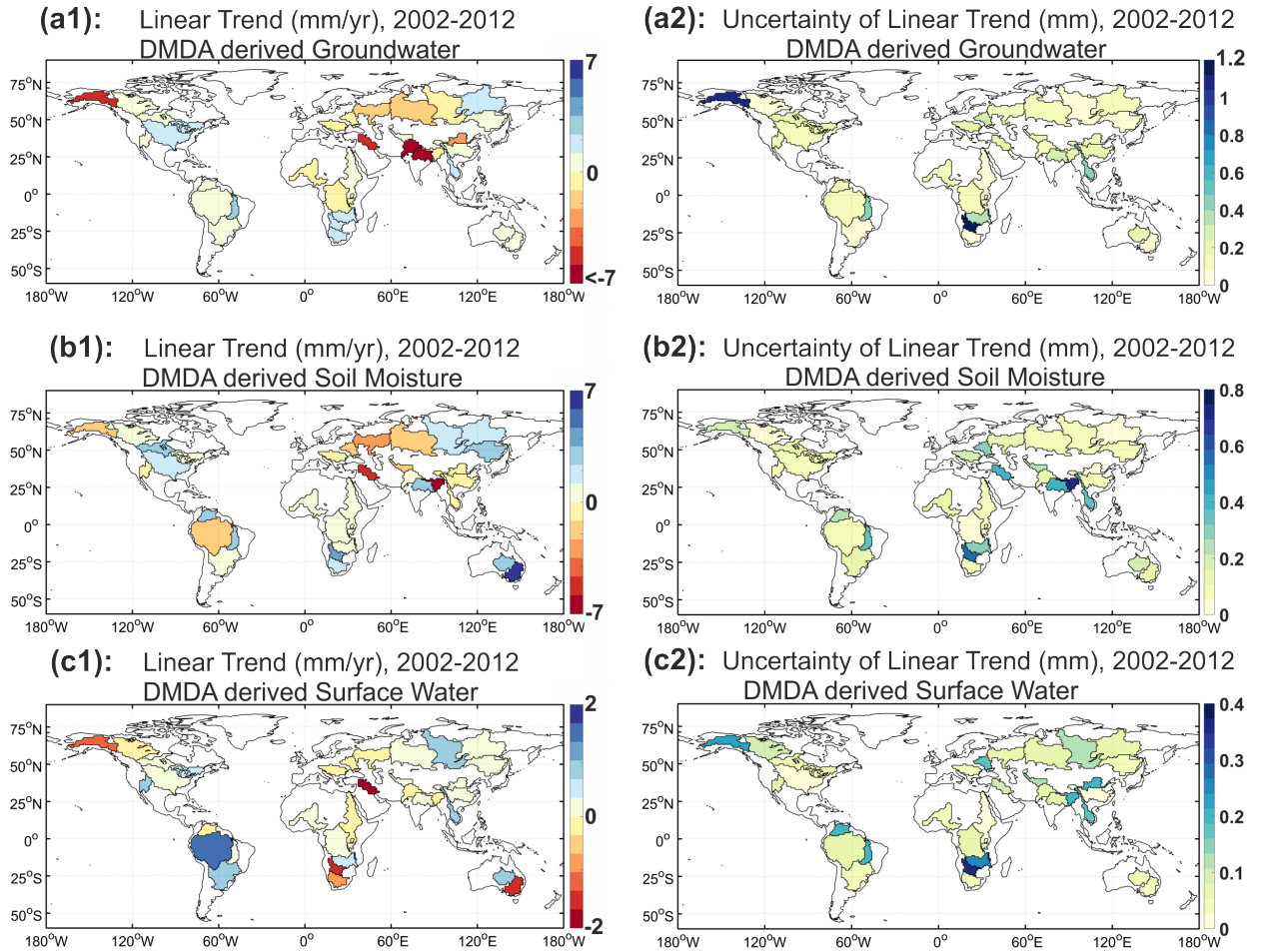


Figure 4: Long-term (2002–2012) linear trend in the DMDA-derived groundwater (a1), soil moisture (b1), and surface water (c1) components, expressed in mm/yr. The uncertainty of these fitted linear trends are shown in (a2), (b2), (c2) respectively.

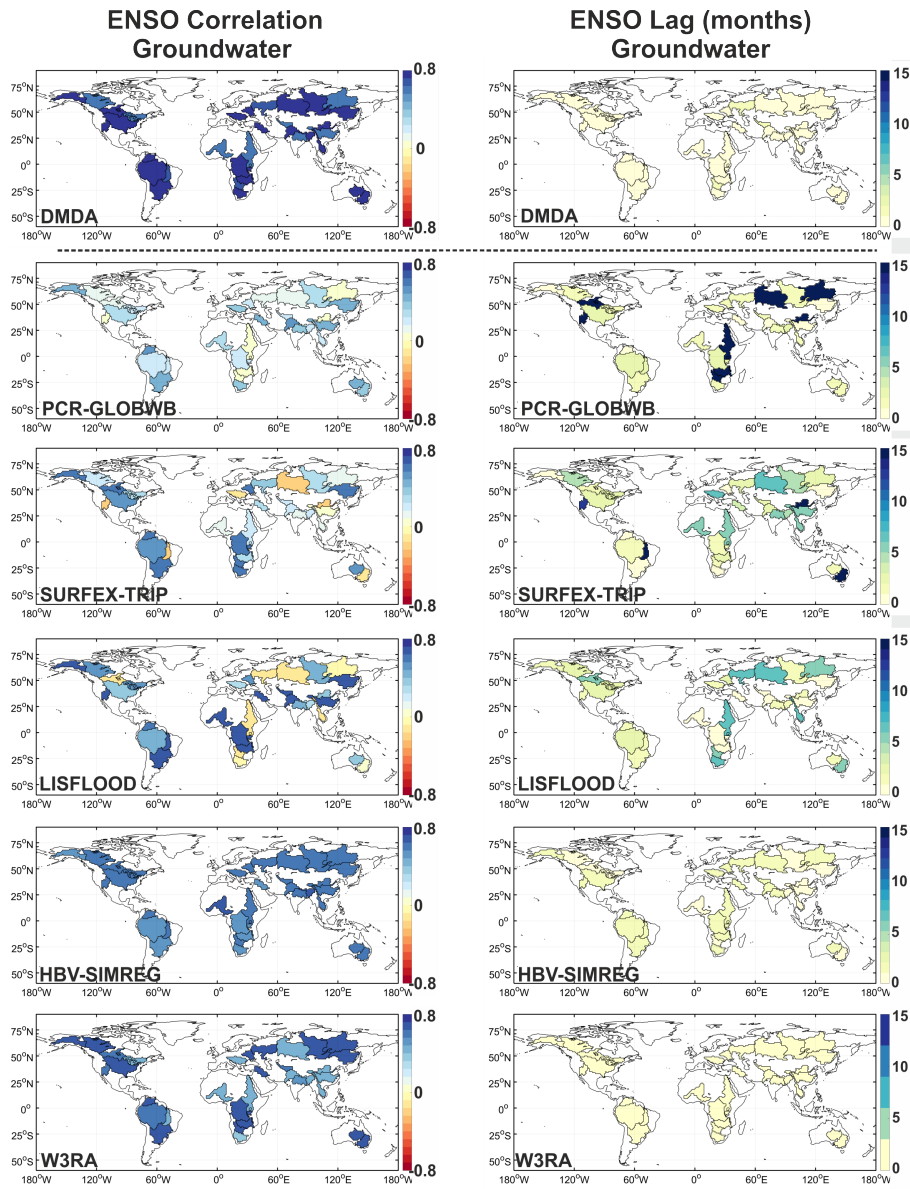


Figure 5: Correlation coefficients and their lags between the ENSO (-Niño 3.4 index) and groundwater estimates derived from the DMDA method and hydrological models used in this study for the period of 2002–2012.

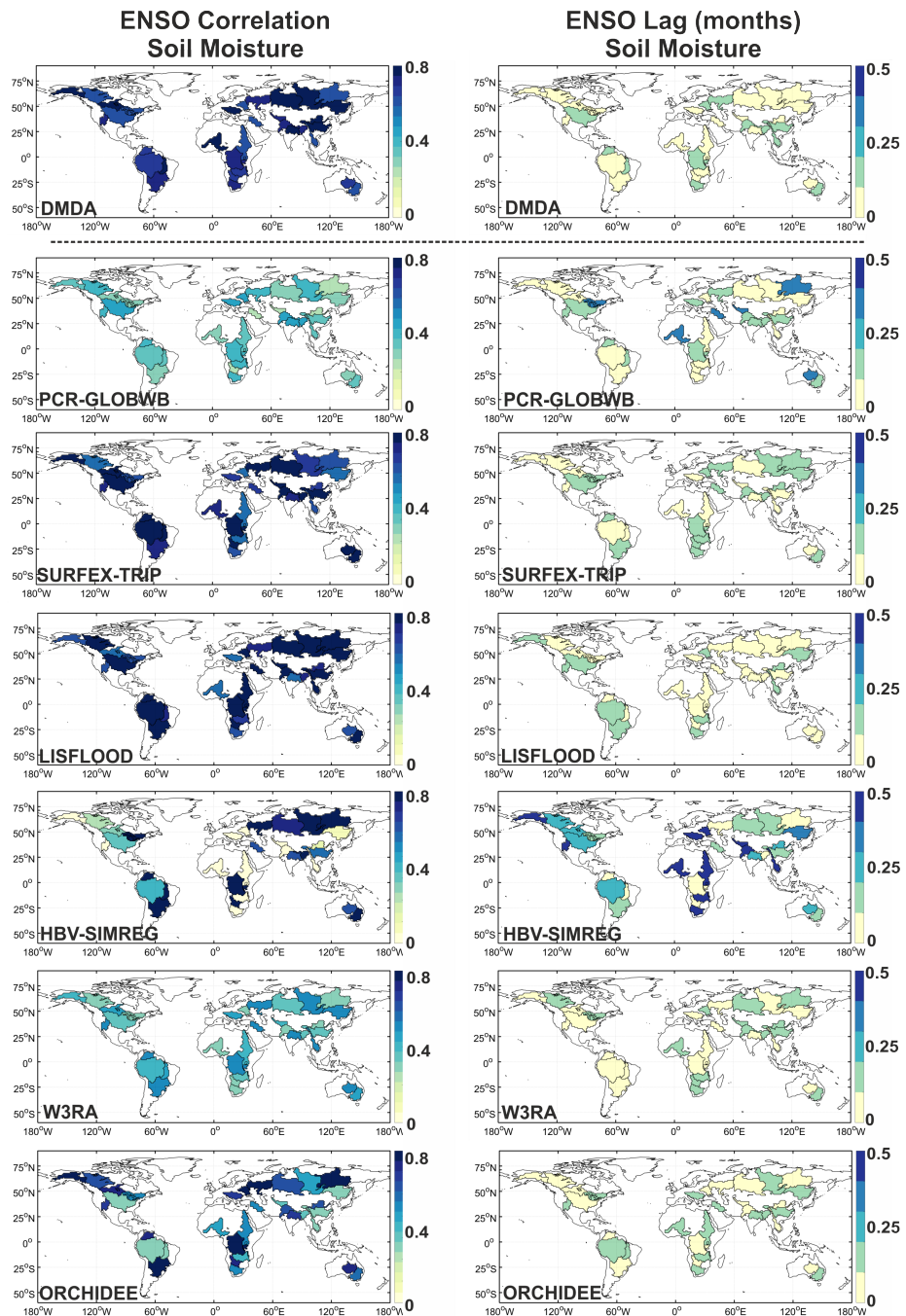


Figure 6: Correlation coefficients and their lags between the ENSO (-Niño 3.4 index) and soil moisture estimates derived from the DMDA method and hydrological models used in this study for the period of 2002–2012.

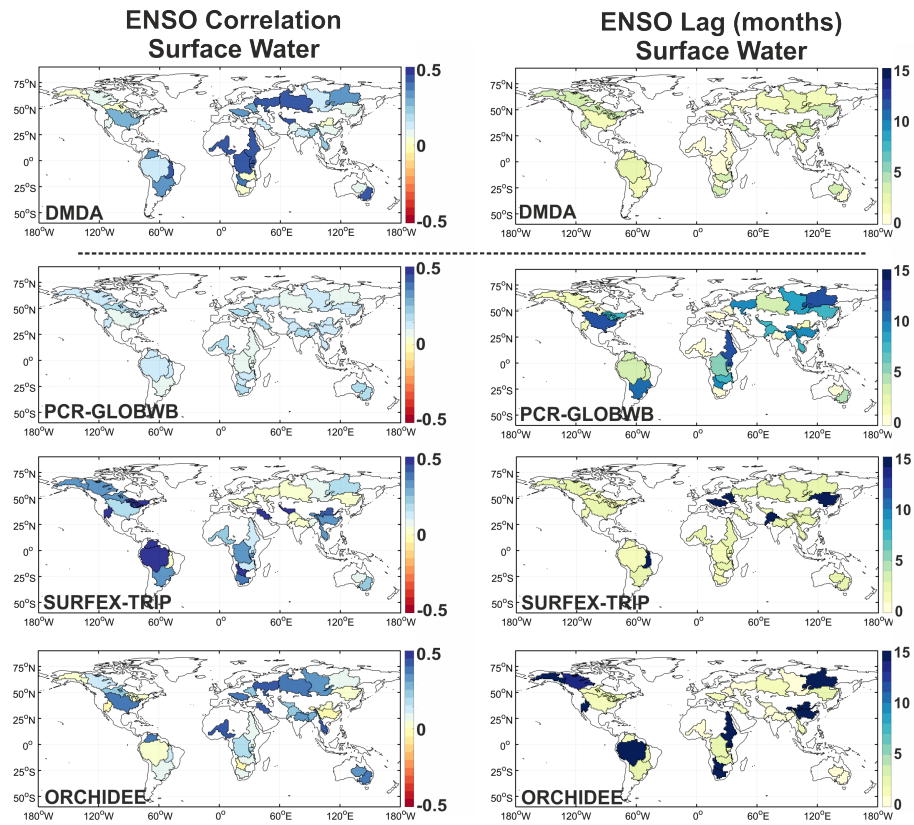


Figure 7: Correlation coefficients and their lags between the ENSO (-Niño 3.4 index) and surface water estimates derived from the DMDA method and hydrological models used in this study for the period of 2002–2012.

Table 1: Overview of models used in this study and their water storage components.

Model	Water Storage Compartments						
	GroundWater	Soil layer	Surface Water	Canopy	Snow	Snow layer	Water Use
PCR-GLOBWB	Yes	2	Yes	Yes	Yes	1	No
W3RA	Yes	3	No	No	Yes	1	No
HBV-SIMREG	Yes	1	No	No	Yes	1	No
SURFEX-TRIP	Yes	14	Yes	Yes	Yes	12	No
LISFLOOD	Yes	2	No	No	Yes	1	Yes
ORCHIDEE	No	11	Yes	No	Yes	6	irrigation

Table 2: An overview of satellite altimetry observation used to validate DMDA results.

Lake	River Basin	Lake mid point	Latitude range of pass	Satellite pass	Cycle
Nasser	Nile	23.31°N 32.83°E	[22.91°N 23.66°N]	94	48
Tana	Nile	12.11°N 37.40°E	[11.95°N 12.19°N]	94	38
chad	Niger	13.01°N 14.38°E	[12.94°N 13.05°N]	248	25
Kainiji	Niger	10.49°N 4.50°E	[10.40°N 10.50°N]	135	21
Malawi	Zambezi	10.84°S 34.40°E	[12.042°S 9.70°S]	44	4
Tanganyika	Zambezi	6.41°S 29.23°E	[8.44°S 4.461°S]	222	11
Guri	Orinoco	7.37°N 117.12°W	[7.06°N 7.67°N]	152	69
Winnipeg	Nelson	53.18°N 98.21°W	[52.82°N 53.55°N]	195	9
Winnipegosis	Nelson	51.91°N 100.01°W	[51.85°N 52.05°N]	195	17
Erie	St. Lawrence	42.11°N 81.48°W	[41.60°N 42.54°N]	193	45
Ontario	St. Lawrence	43.56°N 77.47°W	[43.35°N 43.83°N]	15	36
Tharthar	Euphrates	33.87°N 43.37°E	[33.75°N 34.00°N]	133	70
Urmia	Euphrates	37.25°N 45.45°E	[37.25°N 37.31°N]	133	4
Chany	Ob	54.96°N 77.33°E	[54.94°N 55.02°N]	5	28

Table 3: Magnitude of simulated predictors, observations, and DMDA results in a controlled synthetic simulation.

Hydrological Compartment	Model name	Min [mm]	Max [mm]	RMS [mm]
Groundwater (First model)	LISFLOOD	-10.5	16.1	7.9
Groundwater (Second model)	SURFEX-TRIP	-12.1	39.8	14.2
Groundwater (Expected value of DMDA)	PCR-GLOBWB	-39.5	70.4	24.2
Groundwater (DMDA result)	DMDA Output	-35.3	92.3	19.9
Groundwater (BMA result)	BMA Output	-46.0	130.2	43.8
Soil Moisture (First model)	LISFLOOD	-37.4	62.2	30.8
Soil Moisture (Second model)	SURFEX-TRIP	-45.7	79.9	41.5
Soil Moisture (Expected value of DMDA)	PCR-GLOBWB	-52.0	107.9	48.7
Soil Moisture (DMDA result)	DMDA Output	-58.5	113.8	51.2
Soil Moisture (BMA result)	BMA Output	-40.8	49.6	21.0
TWS (First model)	LISFLOOD	-46.8	75.5	37.2
TWS (Second model)	SURFEX-TRIP	-57.6	115.2	54.6
TWS (Expected value of DMDA results)	PCR-GLOBWB	-83.3	164.5	64.2
TWS (DMDA result)	DMDA Output	-77.8	153.8	63.2
TWS (BMA result)	BMA Output	-77.8	153.8	63.2
$ \Delta _{\text{Groundwater}}$	$ \text{LISFLOOD} - \text{Expected value} $	0	58.1	11.2
$ \Delta _{\text{Groundwater}}$	$ \text{SURFEX} - \text{Expected value} $	0	45.8	10.3
$ \Delta _{\text{Groundwater}}$	$ \text{DMDA} - \text{Expected value} $	0	31.2	5.3
$ \Delta _{\text{Groundwater}}$	$ \text{BMA} - \text{Expected value} $	0	87.6	20.4
$ \Delta _{\text{Soil Moisture}}$	$ \text{LISFLOOD} - \text{Expected value} $	0	46.8	9.6
$ \Delta _{\text{Soil Moisture}}$	$ \text{SURFEX} - \text{Expected value} $	0	29.3	5.7
$ \Delta _{\text{Soil Moisture}}$	$ \text{DMDA} - \text{Expected value} $	0	29.2	5.2
$ \Delta _{\text{Soil Moisture}}$	$ \text{BMA} - \text{Expected value} $	0	89.5	18.6
$ \Delta _{\text{TWS}}$	$ \text{LISFLOOD} - \text{Expected value} $	0	94.7	18.6
$ \Delta _{\text{TWS}}$	$ \text{SURFEX} - \text{Expected value} $	0	60.9	14.1
$ \Delta _{\text{TWS}}$	$ \text{DMDA} - \text{Expected value} $	0	24.2	6.2
$ \Delta _{\text{TWS}}$	$ \text{BMA} - \text{Expected value} $	0	31.4	8.4

Table 4: The amplitude of linear trend [mm/yr] and its uncertainty, fitted to the DMDA-derived groundwater, soil Moisture, and surface water, during 2002–2012.

ID	Basin	DMDA GroundWater	DMDA Soil Moisture	DMDA Surface Water
	Name			
1	Amazon	0.17 ± 0.12	-1.92 ± 0.09	1.43 ± 0.06
2	Amur	0.46 ± 0.06	2.61 ± 0.09	0.25 ± 0.03
3	Aral	0.02 ± 0.08	-1.43 ± 0.22	0.21 ± 0.12
4	Brahmaputra	-0.44 ± 0.16	-7.00 ± 0.69	-0.13 ± 0.21
5	Caspian-Volga	-2.06 ± 0.15	-2.98 ± 0.16	-0.02 ± 0.07
6	Colorado	0.80 ± 0.11	-0.75 ± 0.09	0.82 ± 0.08
7	Congo	-0.72 ± 0.08	0.59 ± 0.03	0.06 ± 0.06
8	Danube	-0.47 ± 0.18	-0.75 ± 0.21	-0.08 ± 0.04
9	Dnieper	-0.5 ± 0.29	-2.27 ± 0.28	-0.03 ± 0.18
10	Euphrates	-5.36 ± 0.23	-5.75 ± 0.39	-2.09 ± 0.09
11	Lake Eyre	0.55 ± 0.16	2.42 ± 0.19	0.77 ± 0.04
12	Ganges	-14.77 ± 0.25	2.69 ± 0.40	0.29 ± 0.05
13	Indus	-8.26 ± 0.16	1.10 ± 0.13	-0.06 ± 0.07
14	Lena	1.74 ± 0.11	1.94 ± 0.05	0.20 ± 0.08
15	Mackenzie	0.51 ± 0.06	0.12 ± 0.05	-0.05 ± 0.10
16	Mekong	1.58 ± 0.43	-0.79 ± 0.33	0.83 ± 0.17
17	Mississippi	1.25 ± 0.09	1.36 ± 0.09	0.33 ± 0.02
18	Murray	0.06 ± 0.06	6.66 ± 0.15	-1.47 ± 0.04
19	Nelson	0.70 ± 0.18	2.45 ± 0.15	0.11 ± 0.03
20	Niger	-1.14 ± 0.15	0.75 ± 0.15	0.32 ± 0.05
21	Nile	0.45 ± 0.06	0.77 ± 0.06	-0.05 ± 0.02
22	Ob	-1.42 ± 0.08	-1.54 ± 0.06	0.05 ± 0.07
23	Okavango	1.74 ± 1.31	3.92 ± 0.55	-1.42 ± 0.37
24	Orange	1.32 ± 0.05	1.28 ± 0.06	-0.85 ± 0.05
25	Orinoco	0.87 ± 0.11	3.45 ± 0.26	-0.22 ± 0.19
26	Parana	0.68 ± 0.08	0.03 ± 0.13	1.04 ± 0.04
27	St. Lawrence	1.49 ± 0.18	1.07 ± 0.07	0.48 ± 0.05
28	Tocantins	2.41 ± 0.47	2.37 ± 0.35	0.08 ± 0.21
29	Yangtze	0.55 ± 0.23	-0.30 ± 0.09	0.20 ± 0.02
30	Yellow	-3.50 ± 0.14	-0.27 ± 0.05	0.08 ± 0.21
31	Yenisei	-0.26 ± 0.07	1.79 ± 0.06	0.75 ± 0.11
32	Yukon	-4.73 ± 1.08	-1.52 ± 0.20	-1.11 ± 0.23
33	Zambezi	1.19 ± 0.38	0.65 ± 0.31	0.35 ± 0.25

Table 5: Correlation between satellite altimetry observation and: I) TWS , II) Surface Water (SW) derived from GRACE, DMDA, and individual models, during 2002–2012.

Basin	Water storage	Correlation between Altimetry Obs. and:							
		GRACE	DMDA	PCR-GLOBWB	SURFEX-TRIP	LISFLOOD	HBV-SIMREG	W3RA	ORCHIDEE
Nile (Nasser Lake)	TWS	0.358	<b>0.381</b>	0.326	0.239	0.095	-0.082	0.001	0.180
	SW	-	<b>0.462</b>	0.363	0.441	-	-	-	-0.046
Nile (Tana Lake)	TWS	0.682	<b>0.718</b>	0.602	0.569	0.517	0.302	0.231	0.635
	SW	-	0.492	0.340	<b>0.603</b>	-	-	-	0.455
St. Lawrence (Erie Lake)	TWS	<b>0.353</b>	<b>0.261</b>	0.271	0.010	-0.121	-0.114	-0.087	-0.010
	SW	-	0.432	<b>0.483</b>	0.126	-	-	-	0.227
St. Lawrence (Ontario Lake)	TWS	<b>0.410</b>	<b>0.364</b>	0.353	0.110	-0.063	-0.064	-0.023	0.037
	SW	-	<b>0.582</b>	0.572	0.273	-	-	-	0.239
Euphrates (Tharthar Lake)	TWS	<b>0.698</b>	<b>0.569</b>	0.225	0.021	0.103	-0.057	0.043	0.182
	SW	-	<b>0.236</b>	0.127	0.093	-	-	-	-0.282
Euphrates (Urmia Lake)	TWS	<b>0.737</b>	<b>0.628</b>	0.223	0.080	0.148	0.021	0.095	0.185
	SW	-	<b>0.172</b>	0.170	0.131	-	-	-	-0.325
Ob (Chany Lake)	TWS	0.393	<b>0.482</b>	0.371	0.303	0.336	0.338	0.348	0.328
	SW	-	<b>0.296</b>	0.278	0.177	-	-	-	-0.333
Zambezi (Malawi Lake)	TWS	0.552	<b>0.632</b>	0.362	0.277	0.346	0.225	0.246	0.391
	SW	-	0.382	0.247	<b>0.410</b>	-	-	-	0.394
Zambezi (Tanganyika Lake)	TWS	<b>0.414</b>	<b>0.365</b>	0.231	0.192	0.121	0.117	0.128	0.160
	SW	-	<b>0.243</b>	0.096	0.241	-	-	-	-0.093
Niger (Chad Lake)	TWS	<b>0.576</b>	<b>0.558</b>	0.436	0.318	0.308	0.065	0.188	0.519
	SW	-	0.657	0.511	0.616	-	-	-	<b>0.689</b>
Niger (Kainiji Lake)	TWS	<b>0.132</b>	<b>0.102</b>	-0.002	-0.149	-0.174	-0.383	-0.278	0.079
	SW	-	<b>0.282</b>	0.126	0.200	-	-	-	0.214
Orinoco (Guri Lake)	TWS	<b>0.585</b>	<b>0.539</b>	0.332	0.427	0.431	0.321	0.301	0.434
	SW	-	<b>0.421</b>	0.314	0.390	-	-	-	0.318
Nelson (Winnipeg Lake)	TWS	<b>0.285</b>	<b>0.270</b>	0.139	-0.185	-0.444	-0.440	-0.389	-0.279
	SW	-	<b>0.104</b>	-0.290	0.072	-	-	-	0.012
Nelson (Winnipegosis Lake)	TWS	0.216	<b>0.249</b>	0.238	0.135	-0.09	-0.164	-0.088	-0.065
	SW	-	<b>0.098</b>	-0.321	-0.015	-	-	-	-0.480